LAPPEENRANTA UNIVERSITY OF TECHNOLOGY
LUT School of Energy Systems
LUT Mechanical Engineering

Qasim Khadim

REAL TIME SIMULATION OF THE COUNTERBALANCE FORKLIFTER WITH MEVEA SOFTWARE

Examiner(s): Professor Aki Mikkola
D.Sc. (Tech.) Kimmo Kerkkänen
LUT School of Energy Systems
Lappeenranta University of Technology
Finland

ABSTRACT

Lappeenranta University of Technology
LUT School of Energy Systems
LUT Mechanical Engineering

Qasim Khadim

REAL TIME SIMULATION OF THE COUNTERBALANCE FORKLIFTER WITH MEVEA SOFTWARE

Master thesis

2017

53 Pages and 31 Figures

Examiner: Professor Aki Mikkola
D.Sc. (Tech.) Kimmo Kerkkänen
LUT School of Energy Systems
Lappeenranta University of Technology
Finland

Keywords: Virtual prototype, Real time simulation, Forklift, Mevea, Multibody system, Product development

In traditional product development approaches, physical prototypes are manufactured many times before the launch of actual product. Mechanical tests generally lead physical prototypes to failure due to inadequate selection of technical aspects and features of products. Conventionally product development methods consume huge amount of time, effort and money. This study deals with real time simulation of counterbalance forklift using Mevea software.

Literature review of research contains a detailed information of components and working of forklift and mathematical equations needed in modelling. Simulated counterbalance truck is to be built on Mevea software in such a way so that the model would be comparable to actual 3 wheel drive 2.0 ton forklift visually and graphically. User feelings such as speed, speed reduction around a curve, mast wobbling, loading lifting capacity of the model, and vibrations during lift will be added to simulation. Simulation model is to be controlled with

G 29 racing wheel and joystick. In order to achieve more realistic behaviors, simulated model will be shifted to simulator. Mevea model will be attached to Simulink for optimizing the results. The results of simulation will be compared to physical prototype tests.

It is expected that developed model would run the simulation in real time. The results of simulation will be close to reference forklift. The behavior of virtual model will also be identical to actual forklift in terms of user feelings on simulator. Mevea truck model would enable to make changes in design quickly and with little effort as compared to physical prototype. Generated model could be further used for R&D purpose and hence, will shorten product development cycle time, cost and effort.

ACKNOWLEDGEMENTS

First of all, I would like to offer gratitude to my parents who had encouraged and supported me during tough patches of my life. I am grateful to my supervisors Professor Aki Mikkola, Tero Hukkataival and Kimmo Kerkkänen about thesis topic, support and constructive feedback. Special thanks to Esa Pekka Kaikko, who was always happy to help me whenever I felt difficulties in my thesis. I appreciate Mevea support and fellow project members with whom I could get discuss issues in my work.

Finally, I want to thank LUT for the opportunity to study mechanical engineering in the progressive and modern university and to open my mind.

Qasim Khadim

Qasim Khadim

Lappeenranta 28.8.2017

TABLE OF CONTENTS

LIST OF SYMBOLS AND ABBREVIATIONS

$\mathbf{A}_i$ Rotational matrix at body *i*

$\mathbf{A}_{j-1,j}$ Relative rotational matrix between body *j* to body *j*-1

$\dot{\mathbf{A}}_i$ First time derivative of rotational matrix at body *i*

C Damping coefficient

$\mathbf{d}_p$ Distance between two points

d_p Normal magnitude of contact

$\mathbf{F}_n$ Normal contact force

$\bar{\mathbf{G}}_i$ Local velocity transformation matrix between angular velocity between angular velocity and first derivative of Euler parameter of body *i*

$\dot{\bar{\mathbf{G}}}_i$ First time derivative of local velocity transformation matrix between angular velocity and first derivative of Euler parameter of body *i*

g_f Static coefficient of friction

$\mathbf{I}$ Identity matrix

K Coefficients of stiffness

$\mathbf{M}$ Mass matrix

$\mathbf{n}$ Normal vector of contact

$\mathbf{Q}_c$ Vector of velocity dependent terms due to differentiation of constraint equations

$\mathbf{Q}_e$ Vector of generalized forces

$\mathbf{Q}_v$ Vector of quadratic velocity in terms of inertia

$\mathbf{q}$ Vector of generalized coordinates

$\mathbf{q}_i$ Vector of generalized coordinates of body *i*

$\dot{\mathbf{q}}$ Vector of generalized velocity

$\ddot{\mathbf{q}}$ Vector of generalized acceleration

$\mathbf{R}_i$ Position of body reference coordinate system

$\dot{\mathbf{R}}_i$ Velocity of body reference coordinate system

$\ddot{\mathbf{R}}_i$ Acceleration of body reference coordinate system

$R_{i\mathrm{X}}$ Vector component of body reference coordinate of body *i* along X-axis

$R_{i\mathrm{Y}}$ Vector component of body reference coordinate of body *i* along Y-axis

$R_{i\mathrm{Z}}$ Vector component of body reference coordinate of body *i* along Z-axis

$\mathbf{r}_{iP}$	Vector of position of point at body *i* in global system
$\dot{\mathbf{r}}_{iP}$	Vector of velocity of point at body *i* in global system
$\ddot{\mathbf{r}}_{ip}$	Vector of acceleration of point at body *i* in global system
r_w	Radius of tire
t	Time
$\bar{\mathbf{u}}_{iP}$	Vector of position of point at body *i* respect to body reference coordinate
$\tilde{\bar{\mathbf{u}}}_{iP}$	Skew symmetric matrix of position vector of point *P*
v_{n}	Relative normal velocity of contact
W_{iner}	Work of inertial forces
W_{ext}	Work of external forces
z	Bristle displacement in LuGre friction model
$\boldsymbol{\theta}_{iE}$	Rotational Euler parameter
$\dot{\boldsymbol{\theta}}_{iE}$	First time derivative of rotational Euler parameter
$\ddot{\boldsymbol{\theta}}_{iE}$	Second time derivative of rotational Euler parameter
θ_0	Euler parameter
θ_1	Euler parameter
θ_2	Euler parameter
θ_3	Euler parameter
$\bar{\boldsymbol{\omega}}_i$	Local angular velocity of body *i*
$\tilde{\bar{\boldsymbol{\omega}}}_i$	Skew symmetric matrix of local angular velocity of body *i*
ω_w	Tire angular velocity
μ_c	Normalized Coulomb friction
μ_s	Normalized static friction
σ_0	Rubber longitudinal lumped stiffness
σ_1	Longitudinal lumped damping coefficient
σ_2	Viscous relative damping
ASME	American society of mechanical engineers
BV	Bounding volume
CAD	Computer aided design
R&D	Research and development
VR	Virtual reality

1 INTRODUCTION

Now a day's digital tools such as computer aided design (CAD), finite element analysis, and multibody dynamics softwares applications are being extensively used by the industries at early stages of product development to shorten the innovation cycle time and enhance the efficiencies of design and launching process (Bruno et al., 2008, pp. 620-630). The potential benefit of implementation of digital tools at initial level of product development process could be the replacement of physical prototypes built to evaluate the technical details of the product (Karkee et al., 2010, pp. 83–96).

In the traditional product development approach, customers are interviewed and their opinions are considered very important in rendering technical features to the actual products based upon which physical prototype is made. It can also be seen in figure 1. However, conventional product development techniques might be challenging for customers to understand benefits and pitfalls of a very new product and hence, the end users might not be able to express needs in the final product in terms of technical aspect of the product at very initial phase. Moreover, customer prerequisites and the technical specifications of the products can only be seen after the manufacturing of physical prototype which frequently leads to failure. Therefore, the conventionally applied product development methods in research and development are often expensive, time consuming and do not meet the requirements and end users cannot participate openly in the product development process. (Tiainen, Ellman and Kaapu, 2014, pp. 169-180.)

Figure 1. Conventional product development process

This problem can be solved by designing and simulating the multibody systems on the digital tools such as Mevea which would simulate the product working cycle in real-time and let the users to make changes in the design process quite efficiently and at fast rate for Research and Development (R & D) purposes illustrated in figure 2. Furthermore, it could also provide a chance to research engineers to make very quick changes in the design for the accurate physical prototype and actual product.

Mevea will also allow the customers to take part actively in the design phase and see how the perspectives related to the technical aspects affect the working of a multibody system in the simulation environment. The working and behaviour of machine in the real-time can also be controlled and visualized with the help of virtual reality (VR) tools such as joystick, racing wheel, virtual glasses, leap controller, and simulator. The real-time simulation tools are ultimately much cheaper, and could shorten the product development process quite significantly.

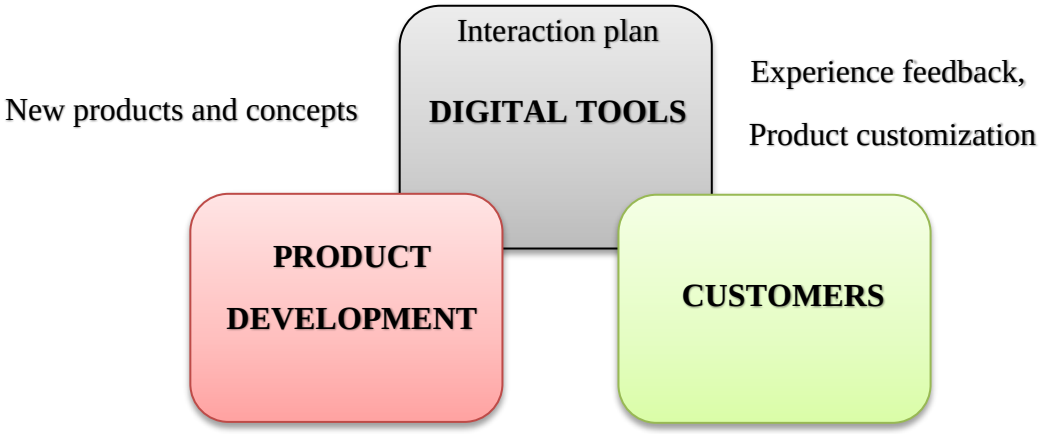

Figure 2. Modern product development approach

1.1 Research background

According to American Society of Mechanical Engineers (ASME), "A powered industrial truck as a power-propelled truck used to carry, push, lift, stack, or tier materials. Powered industrial trucks are also called forklift" (Davis, 2013, p. 1). The modern forklift trucks ensure that daily industrial operations are completed smoothly and in time. Among the various types of forklift models, counterbalance forklift trucks are gaining more importance in the advanced logistic systems due to light weight, comfort, and adaptive speed control system.

In the counterbalance forklift, the weight of carried load is counterbalanced by the rear portion. The weight carrying capacity of forklifter is proportional to the weight of counterbalance. Therefore, the weight carrying capacity of forklift will be high if the counterbalance also has large weight. (Bermejo and Felez, 2016, p. 2.)

To build the simulation model of truck in real-time, it is very important to understand the individual parts, movements and functions. The whole counterbalance forklift could be divided into two units; vehicle body, and mast assembly unit. Figure 3 explains the various components of vehicle body of counterbalance forklift based upon which the functionality of this unit might be interpreted (Hangcha Group, 2011, pp. 59-75).

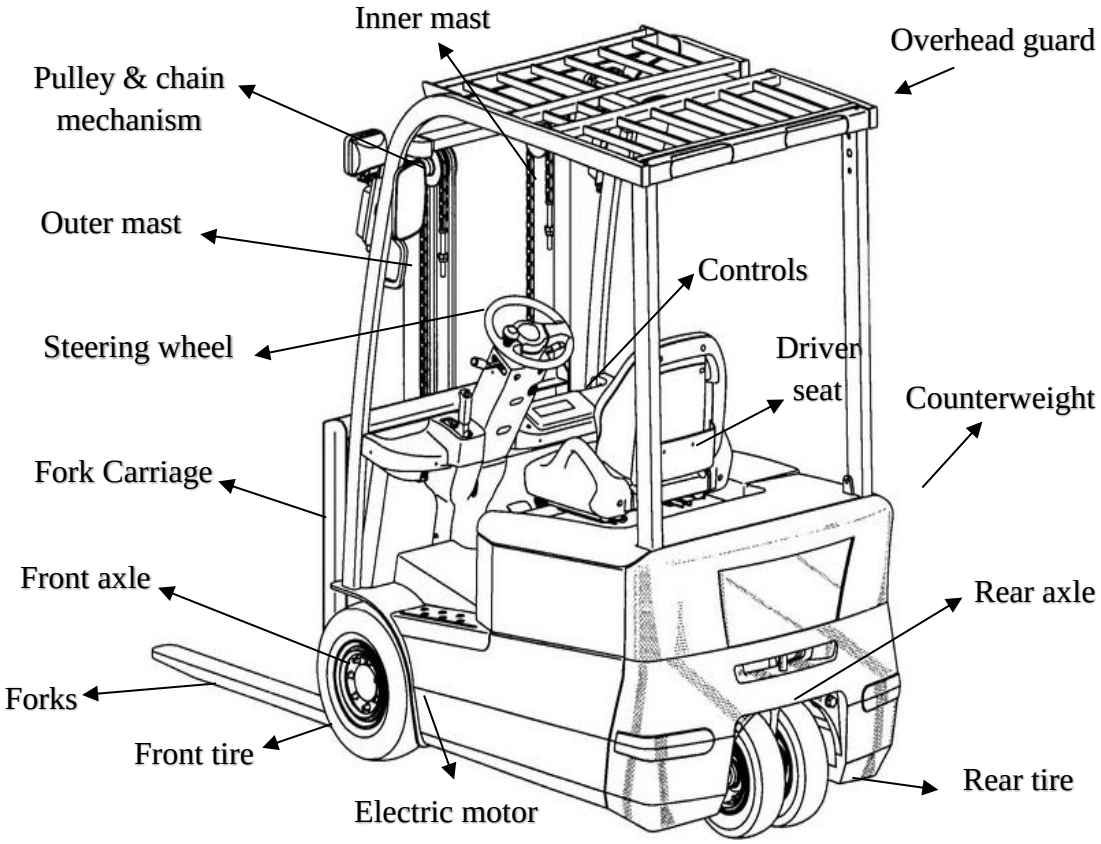

Figure 3. The components of 3W electric counterbalance forklift (Toyota Parts, 2017)

The vehicle portion of electrically powered counterbalance forklift comprises from overhead guard, electric motor, counterweight, rear axle, front axle, gearbox, and tires. Generally, the driving operation is controlled by front axle whereas the steering is regulated with rear axle. The counterbalance forklift model is further equipped with electric motor, clutches, gearbox, differential gears and tires inside vehicle unit body to let the vehicle move and perform

operations. The overhead guard ensures the safety of driver during work. Moreover, the automobile unit is provided with a comfortable driver seat, steering wheel and controls. (Toyota Parts, 2017; Luciano Mondani, Mark Dodd, 2003)

Mast assembly is considered as the complex portion of forklift. It contains outer mast, inner mast, fork carriage and forks. Outermast can be tilted within specific angle range. Inner mast and fork carriage are generally utilized to lift the load in upward and downward directions. However, in few forklifts innermast alone is used for lifting operations and fork carriage is fixed with it. Forks are attached to fork carriage in a way so that it can move loads along sideways. (ProLift, 2017; Luciano Mondani, Mark Dodd, 2003) More detailed information of mast assembly will be described in the late part of study.

In the conventional product development approach, physical prototypes are made in an industrial company either by assembling the already manufactured prototypes or building a completely new prototype. It is further tested to check feasibility and working of product. Mechanical tests often leads to failure as can also be seen in figure 4. For example, if the vehicle unit model is to be tested it would be assembled to previously made mast assembly prototype and the concerned experiments would be performed. However, the possible failure of the newly developed model could also lead to a huge amount of budget, space and time.

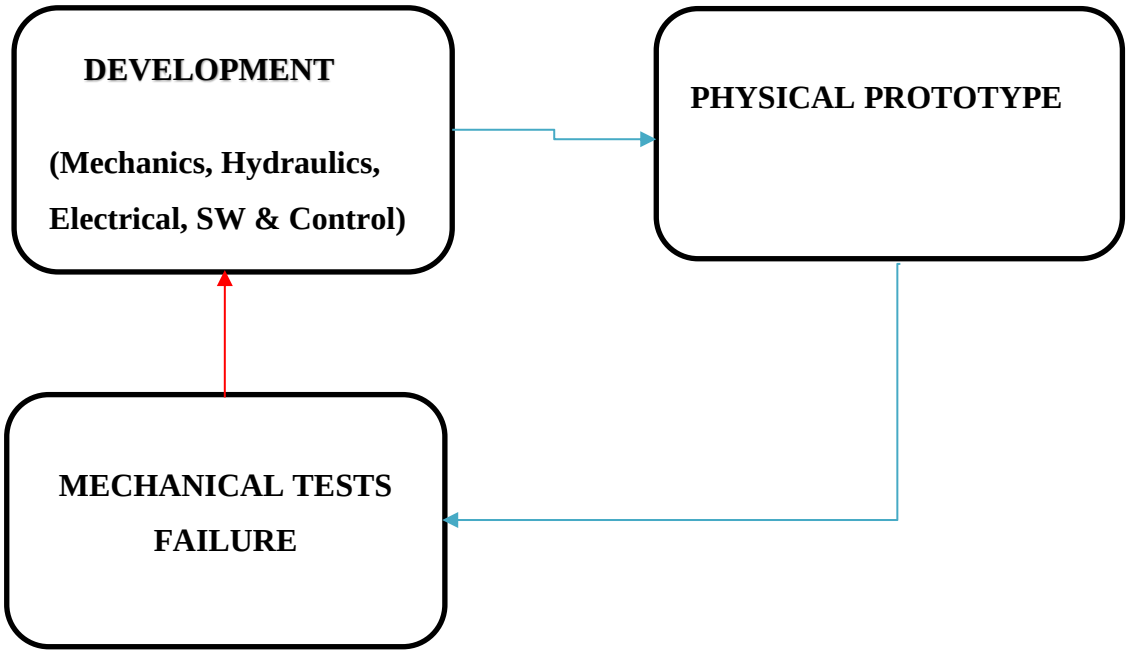

Figure 4. Current product development approach in a manufacturing company

The recent development of real time simulation software Mevea might provide R&D team an extra ordinary digital tool to test, experiment, and simulate the working cycle of forklift in real time before the manufacturing of physical prototype as shown in figure 5 as well. It could run the simulation of machine in real time. Therefore, it could considerably save the money, time and enhance research and development's capabilities of a manufacturing company's capabilities over the competitors.

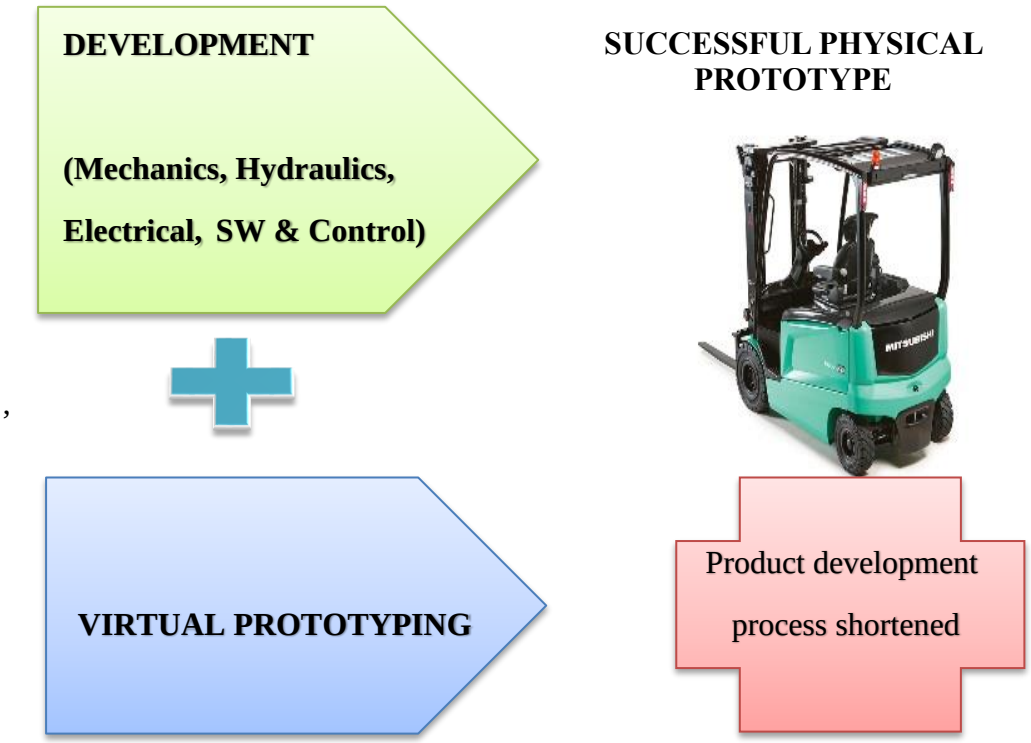

Figure 5. Possible role of real-time simulation software in R&D of industrial company

The aim of this study is to model and simulate electric counterbalance truck by using Mevea simulation software. The simulated counterbalance truck model would have three wheels, 3.5 tons weight and lifting capacity of 2000 Kg. Vehicle movement and steering operations would be replica of actual forklift. Moreover, mast assembly components would execute identical functions as 3 wheel drive 2.0 ton forklift drive. In order to have a realistic simulation and effective results, besides using the Mevea model and multi body dynamics the numerous and complex events in the real world such as environment, collisions, and lights are to be considered. Mevea simulation made on these principles might describe the detailed construction of machine, function of its components, and let to find the potential problems to be faced during working and operation in much better way.

1.2 Research problem and goals

This study focuses on the modeling and simulation the working of an electric counterbalance forklift using multibody dynamics system Mevea software. The simulated forklift model will be used to test and analyze the truck model and its components during operation. The research problem under discussion can be further divided into three research questions which can also be seen in the figure 6.

- Development of an initial forklift Mevea model
- Real time simulation and control of Mevea model
- Attachment of virtual reality tools

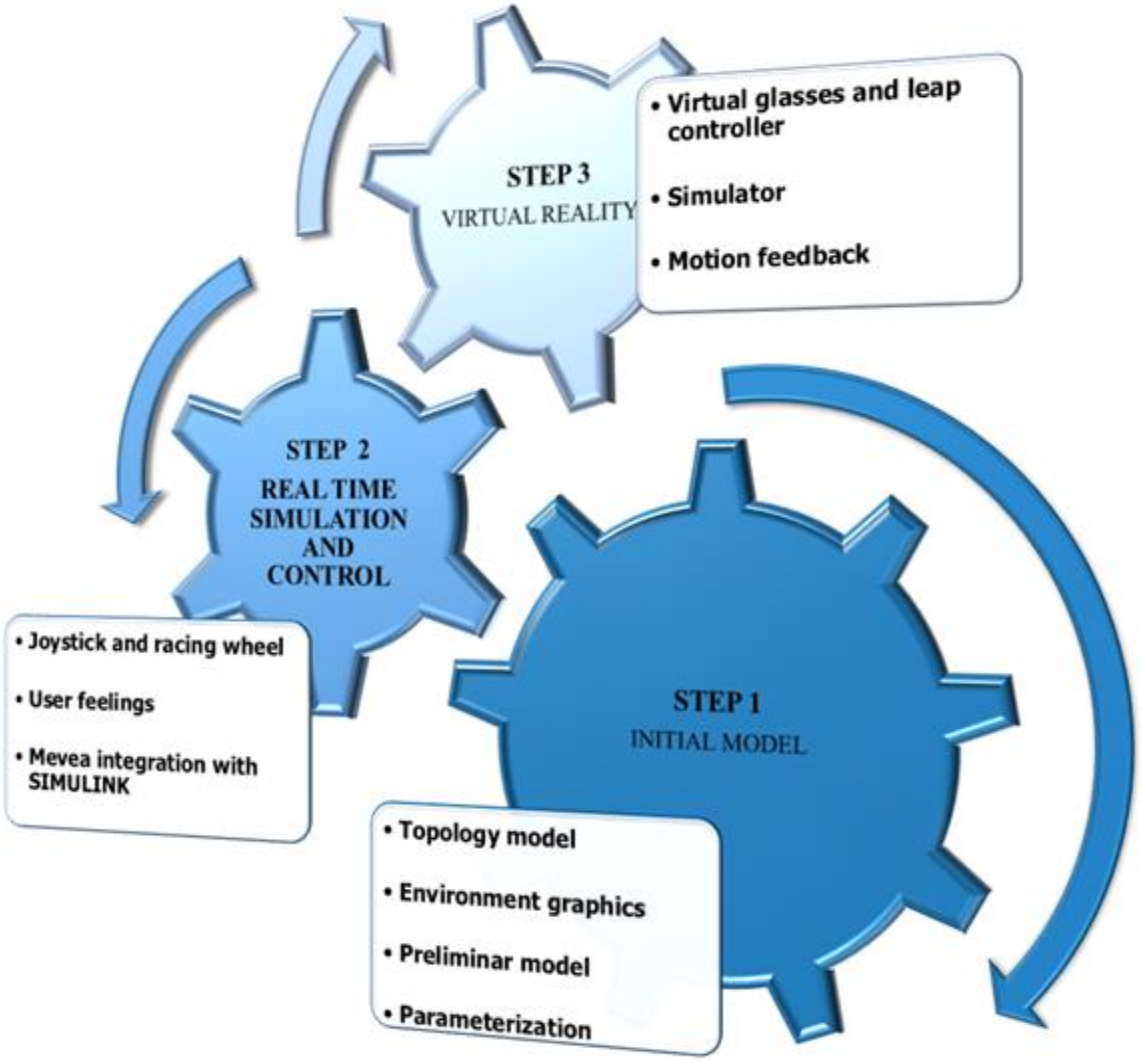

Figure 6. Objectives of the project

1.3 Research methods

In order to solve research questions, both qualitative and quantitative methods will be utilized. First step is to model the forklift on Mevea considering the topology of truck as described in figure 6. Mevea simulation is to be run in an offshore port containing ocean, sky, crane, tilted path, storage area, and containers for loading and unloading purposes. The vehicle model could be run in the actual parameters to asses and compare the performance of vehicle in real time. The second research question will be related to addition of the realistic feelings and control of the simulation as shown in figure 6.

Mevea model would be attached to joystick and racing wheel for purpose of better control and comfort. The vehicle model will be operated by using G29 racing wheel whereas the mast assembly operations could be managed using joystick. In order to test the realistic behavior of the parametrized forklift model, physical phenomenon such as speed, speed reduction around a curve, mast wobbling, loading lifting capacity of the model, and vibrations during lift would be taken into account in the simulation. The forklift model could collide with the walls of storage area, containers and crane like a real vehicle model. The parametrized Mevea model will also be further integrated with Matlab Simulink. The Simulink model will contain the steering system of model having number design features such as motor, gearbox, planet gear and tier model. The co-simulation environment would enhance the user control and optimization for the purpose of better results which could be further used in R&D. As described in the figure 6, the final research question is to add the virtual reality tools in the Mevea simulation. The model will be equipped with virtual glasses and leap controllers to see the simulation environment. Moreover, the forklift Mevea model will be transferred to LUT Sim Studio simulator to get better realistic feelings and test the behavior of all components in real time. Furthermore, motion platform feedback would be added on the simulator in order to experience the vibrations being caused during the movements of forklift on the port.

1.4 Contribution of study

It is expected that the real time simulation of forklift would operate successfully with racing wheel and joystick and the behavior executed by the Mevea model would be similar to the reference forklift. Generated graphs of Mevea simulation of forklift will be comparable to physical prototype. The added user feelings such as maximum speed, speed reduction around

a curve, mast wobbling, loading lifting capacity of the model, and vibrations during lift would be analogous to the actual 3 wheel drive 2.0 ton forklift. The parametrized model could collide with the obstacles and give the actual feelings to the test driver. Simulink co-simulation environment with Mevea would let the users to make the changes in design very quickly and better controllability and optimization.

Attachment of Mevea forklift model with virtual reality tools and motion feedback might ensure the users to experience the virtual test drive in real time and have realistic feelings. In order to compare the simulated vehicle unit, speed, brake and response of steering system of Mevea model will be compared to reference forklift. Working of mast unit will be tested by load lifting capacity, tilt forward and backward, fork and inner mast lifting speeds under many loads. Graphs of mentioned features would be matched with the physical prototype testing results. It could be anticipated that Mevea simulation would run the simulation in real time and the generated results would be similar in terms of visualization effects of user feelings and graphical results. The running of simulation on Mevea software might also be used to simulate, tests, and validates the truck lift models in future and could save the time and prototype manufacturing cost of the product.

2 MULTIBODY SYSTEM FORMULATIONS

The equations of motion for the forklift simulation might be solved using numerical time integration methods. The constraint equations of motion based upon virtual work could be further used to find out the dynamic equilibrium of the multibody system. The kinematics system can be explained using global formulation. The kinematics of multibody forklift system help to determine the equation of motion. The coordinates of bodies are described with respect global frame of reference in the global formulation.

2.1 Kinematics

Figure 7 represents a rigid body *i* in the *XYZ* global coordinate system. The point *P* located on the rigid body *i* is described by body coordinate system *xyz*. The vector $\bar{\mathbf{u}}_{iP}$ shown in figure 7 is the position of point *P* in the body reference coordinate system *xyz*.

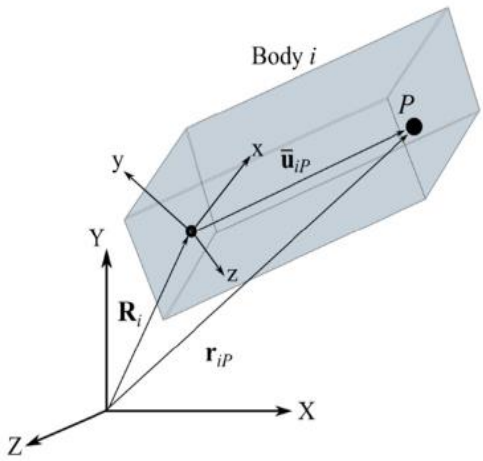

Figure 7. The position of point *P* on the rigid body *i* (Baharudin, 2016, pp.24-43)

The global position $\mathbf{r}_{iP}$ of point *P* on the body *i* can be written using the following equation:

$$\mathbf{r}_{iP} = \mathbf{R}_i + \mathbf{A}_i \bar{\mathbf{u}}_{iP} \tag{1}$$

Where, $\mathbf{R}_i$ describes the position of the body reference coordinate system relative to *XYZ* global coordinate system, and $\mathbf{A}_i$ is the rotation matrix representing the orientation of body

i with respect to global coordinate system *XYZ*. The generalized coordinates $\mathbf{q}_i$ of a rigid body can be written as:

$$\mathbf{q}_i = \begin{bmatrix} \mathbf{R}_i{}^{\mathrm{T}} & \boldsymbol{\theta}_{iE}^{\mathrm{T}} \end{bmatrix}^{\mathrm{T}} \tag{2}$$

In equation 2, $\mathbf{R}_i = [R_{i\mathrm{X}} \quad R_{i\mathrm{Y}} \quad R_{i\mathrm{Z}}]^{\mathrm{T}}$ is the origin of body reference coordinate system and $\boldsymbol{\theta}_{iE}$ is a direction vector of rotational coordinate system which can be represented as:

$$\boldsymbol{\theta}_{iE} = [\theta_0 \quad \theta_1 \quad \theta_2 \quad \theta_3]^{\mathrm{T}} \tag{3}$$

θ_0, θ_1, θ_2 and θ_3 are known as Euler parameters. The rotation matrix $\mathbf{A}_i$ can be described using Euler parameters as:

$$\mathbf{A}_i = \begin{bmatrix} 1-2\theta_2^2-2\theta_3^2 & 2(\theta_1\theta_2-\theta_0\theta_3) & 2(\theta_1\theta_3+\theta_0\theta_2) \\ 2(\theta_1\theta_2+\theta_0\theta_3) & 1-2\theta_1^2-2\theta_3^2 & 2(\theta_2\theta_3+\theta_0\theta_1) \\ 2(\theta_1\theta_3-\theta_0\theta_2) & 2(\theta_2\theta_3+\theta_0\theta_1) & 1-2\theta_1^2-2{\theta_2}^2 \end{bmatrix}_i \tag{4}$$

Euler parameters describe the following mathematical constraint equation which must be fulfilled:

$$\boldsymbol{\theta}_{iE}^T \boldsymbol{\theta}_{iE} - 1 = 0 \tag{5}$$

The velocity of point *P* on rigid body *i* can be obtained by differentiating equation (1) with respect to time and can be written as:

$$\dot{\mathbf{r}}_{iP} = \dot{\mathbf{R}}_i + \dot{\mathbf{A}}_i \bar{\mathbf{u}}_{iP} \tag{6}$$

$$\dot{\mathbf{r}}_{iP} = \dot{\mathbf{R}}_i - \dot{\mathbf{A}}_i \tilde{\bar{\mathbf{u}}}_{iP} \bar{\boldsymbol{\omega}}_i \tag{7}$$

where $\dot{\mathbf{R}}_i$ is the derivative of vector of the body coordinate system relative to coordinate system, $\dot{\mathbf{A}}_i$ is the derivative of rotation matrix, $\tilde{\bar{\mathbf{u}}}_{iP}$ is skew-symmetric matrix of vector $\bar{\mathbf{u}}_{iP}$ and $\bar{\boldsymbol{\omega}}_i$ is angular speed. The angular speed $\bar{\boldsymbol{\omega}}_i$ can be written as:

$$\bar{\boldsymbol{\omega}}_i = \bar{\mathbf{G}}_i \dot{\boldsymbol{\theta}}_{iE} \tag{8}$$

$\dot{\boldsymbol{\theta}}_{iE}$ is the derivative of Euler parameter and $\bar{\mathbf{G}}_i$ local transformation matrix related to global and local component of body *i* which can be described as Euler parameters:

$$\bar{\mathbf{G}}_i = \begin{bmatrix} -\theta_1 & \theta_0 & \theta_3 & -\theta_2 \\ -\theta_2 & -\theta_3 & \theta_0 & \theta_1 \\ -\theta_3 & \theta_2 & -\theta_1 & \theta_0 \end{bmatrix}_i \tag{9}$$

The velocity vector $\dot{\mathbf{r}}_{iP}$ can be explained in terms generalized coordinate system as:

$$\dot{\mathbf{r}}_{iP} = [\mathbf{I} \quad -\mathbf{A}_i \, \tilde{\bar{\mathbf{u}}}_{iP} \, \bar{\mathbf{G}}_i] \begin{bmatrix} \dot{\mathbf{R}}_i \\ \dot{\boldsymbol{\theta}}_{iE} \end{bmatrix} \tag{10}$$

In the above equation, **I** is 3x3 identity matrix. The acceleration vector $\ddot{\mathbf{r}}_{ip}$ of point *P* can be obtained by differentiating the equation 10 with respect to time. It can be explained mathematically as:

$$\ddot{\mathbf{r}}_{ip} = [\mathbf{I} \quad -\mathbf{A}_i \, \tilde{\bar{\mathbf{u}}}_{iP} \, \bar{\mathbf{G}}_i] \begin{bmatrix} \ddot{\mathbf{R}}_i \\ \ddot{\boldsymbol{\theta}}_{iE} \end{bmatrix} + \begin{bmatrix} 0 & \mathbf{A}_i \, \tilde{\bar{\boldsymbol{\omega}}}_i \tilde{\bar{\mathbf{u}}}_{iP} \, \bar{\mathbf{G}}_i - \mathbf{A}_i \, \tilde{\bar{\mathbf{u}}}_{iP} \, \dot{\bar{\mathbf{G}}}_i \end{bmatrix} \begin{bmatrix} \dot{\mathbf{R}}_i \\ \dot{\boldsymbol{\theta}}_{iE} \end{bmatrix} \tag{11}$$

In the equation 11, $\ddot{\mathbf{q}}_i = [\ddot{\mathbf{R}}_i \quad \ddot{\boldsymbol{\theta}}_{iE}]$ represents generalized acceleration containing $\ddot{\mathbf{R}}_i$ second derivative of position of body *i* with respect to *XYZ* global coordinate system, $\ddot{\boldsymbol{\theta}}_{\boldsymbol{iE}}$ second derivative of Euler parameters; $\tilde{\bar{\boldsymbol{\omega}}}_i$ is the skew symmetric matrix of angular velocity and $\dot{\bar{\mathbf{G}}}_i$ is the first time derivative of the local transformation matrix.

2.2 Equation of motion

The equation of motion condition is obtained using the concept of virtual work and the principle of least motion. The dynamic equilibrium of a multibody system can be developed by equalizing the virtual work done by inertial and external forces in an unconstrained system.

$$\delta W_{iner} = \delta W_{ext} \tag{12}$$

In the equation 12, δW_{iner} represents the virtual work done by inertial forces whereas δW_{ext} is the virtual work done by externally applied forces. The work done by the virtual forces can be written mathematically as:

$$\delta W_{iner} = \delta \mathbf{q} \,.\, (\mathbf{M\ddot{q}} - \mathbf{Q}_v) \tag{13}$$

$$\delta W_{ext} = \delta \mathbf{q} . \mathbf{Q}_e \tag{14}$$

In the equation (13) and (14), **M** is the mass matrix, $\ddot{\mathbf{q}}$ is the generalized accelerations, $\mathbf{Q}_v$ is the vector of quadratic velocity vector and $\mathbf{Q_e}$ is the vector of generalized forces of a body. For a constrained multibody system, the equation of motion described in equation (12) can be written as:

$$\delta \mathbf{q} \,.\, (\mathbf{M\ddot{q}} - \mathbf{Q}_v - \mathbf{Q}_e) \neq 0 \tag{15}$$

2.3 Collision and contact modeling

In the forklift Mevea model, the collisions play a very important role in order to get realist user feelings. The parameterized model might collide with the walls of container and obstacles which comes in the path. Therefore, it will be very necessary to determine colliding pair and the effect of collision on forklift body and other pair can also be termed as collision detection and collision response, respectively. (Baharudin, 2016, pp.24-43.)

The collision detection determines the collision at a specific point and time whereas the collision response helps to calculate the contact force between two bodies. The contact model acts as function to find out the collision point and response out of it. The contact model could be evaluated by developing an algorithm illustrated in figure 8. The figure shows that the bounding distance between the pair would decide the collision detection and collision response. (Baharudin, 2016, pp.24-43.)

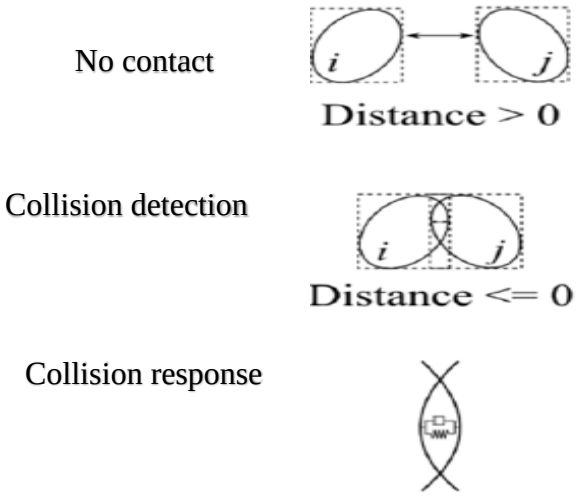

Figure 8. The contact model between colliding pair (Baharudin, 2016, pp.24-43)

The collision detection can be found between two colliding pair by considering two complex geometries in contact. The volume in contact known as bounding volume (BV) is supposed to be in a simple box shape as shown in figure 9. The collision response can be calculated by considering the colliding pair as spring damper system and finding out the depth of penetration. It also contains friction to describe the collision between different types of materials. The contact force caused during the collision expresses the collision detection. (Baharudin, 2016, pp.24-43.)

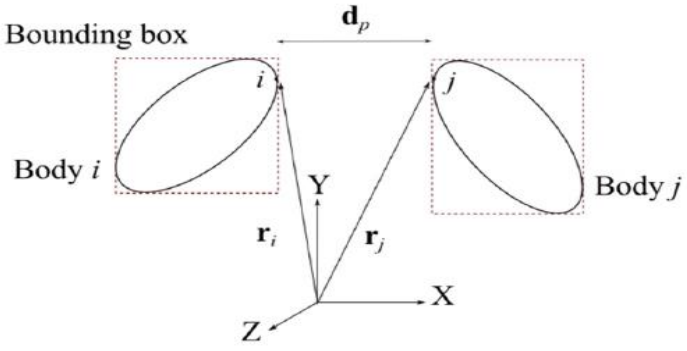

Figure 9. Contact between two bodies (Baharudin, 2016, pp.24-43)

Figure 9 describes two colliding bodies i and j located at $\mathbf{r}_i$ and $\mathbf{r}_j$ with respect to global coordinate system XYZ. Bodies i and j can be treated as bounding box and the penetration distance between two bodies $\mathbf{d}_p$can be calculated as:

$$\mathbf{d}_p = \mathbf{r}_j - \mathbf{r}_i \tag{14}$$

The normal vector of the contact can be calculated as:

$$\mathbf{n} = \frac{\mathbf{d}_p}{\|\mathbf{d}_p\|} \tag{15}$$

The normal magnitude between two points d_p can be determined by combining both the normal vector and penetration distance. Mathematically, it is expressed as:

$$d_p = \mathbf{n}^{\mathrm{T}}\mathbf{d}_p \tag{16}$$

Equation (16) would determine the location of collision and if the time is included the relative velocity v_{n} has to be considered. The relative normal velocity v_{n} can be obtained by differentiating equation (14) with respect to time:

$$v_{\mathrm{n}} = \mathbf{n}^{\mathrm{T}}\left(\dot{\mathbf{r}}_j - \dot{\mathbf{r}}_i\right) \tag{17}$$

In order to find the collision response, the contact force is calculated. A spring damper is added to explain the contact force $\mathbf{F}_n$ at the point of contact and mathematically it is written as:

$$\mathbf{F}_n = -\left(Kd_p + Cv_n\right)\mathbf{n} \tag{18}$$

Where *K* and *C* are the coefficients of stiffness and damping factors and both coefficients play a very important role and decide the collision response. The spring and stiffness contacts values should be carefully chosen.

2.4 The tire model

The tire of vehicle transmit forces between ground and the rim. Mevea Modeler uses Pacejka and LuGre model to compute the tire behavior during simulation. In the discussed Mevea model, LuGre tire model is used to describe tire in motion. The profile of tire in the Mevea model can be explained either by using width and radius or splines. Splines define the shape of tire in more detailed way in Mevea.

A tire can be thought in terms of discs having specific width and radius shown in figure 10a. The disks are supposed to be in a rigid form. As can be seen in figure 10c, forces along x, y and z axis are represented whereas figure 10a illustrates the force between tire and road and normal force. As indicated in figure 10b, this model is based upon the consideration of tire model as an elastic bristle at the microscopic level. The tangential force on the bristle causes it to behave like a spring. When a large amount of tangential force is applied, the bristle starts to slip along longitudinal direction explained in figure 10b. (Baharudin, 2016, pp.24-43.)

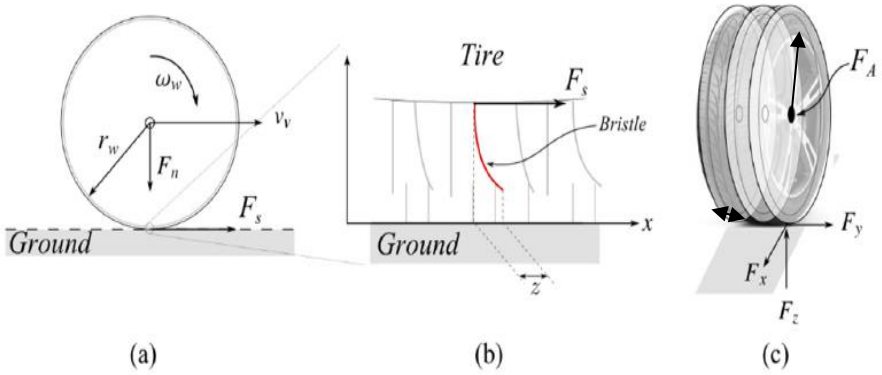

Figure 10. LuGre's tire model (Baharudin, 2016, pp.24-43.)

The bristle is deflected along z axis and the bristle deflection z can be written with respect to time t as:

$$\frac{dz}{dt} = v_r - \frac{\sigma_0 |v_r|}{g_f} z \tag{19}$$

Where v_r is the relative velocity between tire and ground, g_f is the friction and σ_0 is the tire longitudinal friction. The relative velocity v_r is further described as:

$$v_r = r_w \omega_w - v_v \tag{20}$$

In equation (20), r_w is radius, ω_w angular velocity of tire and v_v is the velocity of forklift illustrated in figure 10. The friction force is caused due to transmitting the force between tire and ground. The friction g_f can be explained as:

$$g_f = \mu_c + (\mu_s - \mu_c)e^{-\left|\frac{v_r}{v_s}\right|^{-\frac{1}{2}}} \tag{21}$$

In equation (21) μ_c is normalized Coulomb friction, μ_s is normalized static friction and v_s is Stribeck relative velocity. Friction g_f depends upon temperature, material and other factors. Friction force F_s is:

$$F_s = \left(\sigma_0 z + \sigma_1 \frac{dz}{dt} + \sigma_2 v_r\right) F_n \tag{22}$$

where σ_1 is the longitudinal lumped damping coefficient, σ_2 relative damping and F_n normal force.

3 REAL TIME MODEL OF A FORKLIFT

In this part of study, the step by step approach needed to prepare forklift on Mevea Software will be described. Mevea model tree shown in figure 11 contains the methodology opted to investigate the research questions. As shown in flow diagrams description of working principle of forklift, body components and topology of model, collecting information, environment modeling, vehicle unit and mast assembly, and simulated Mevea model are the main steps of modelling.

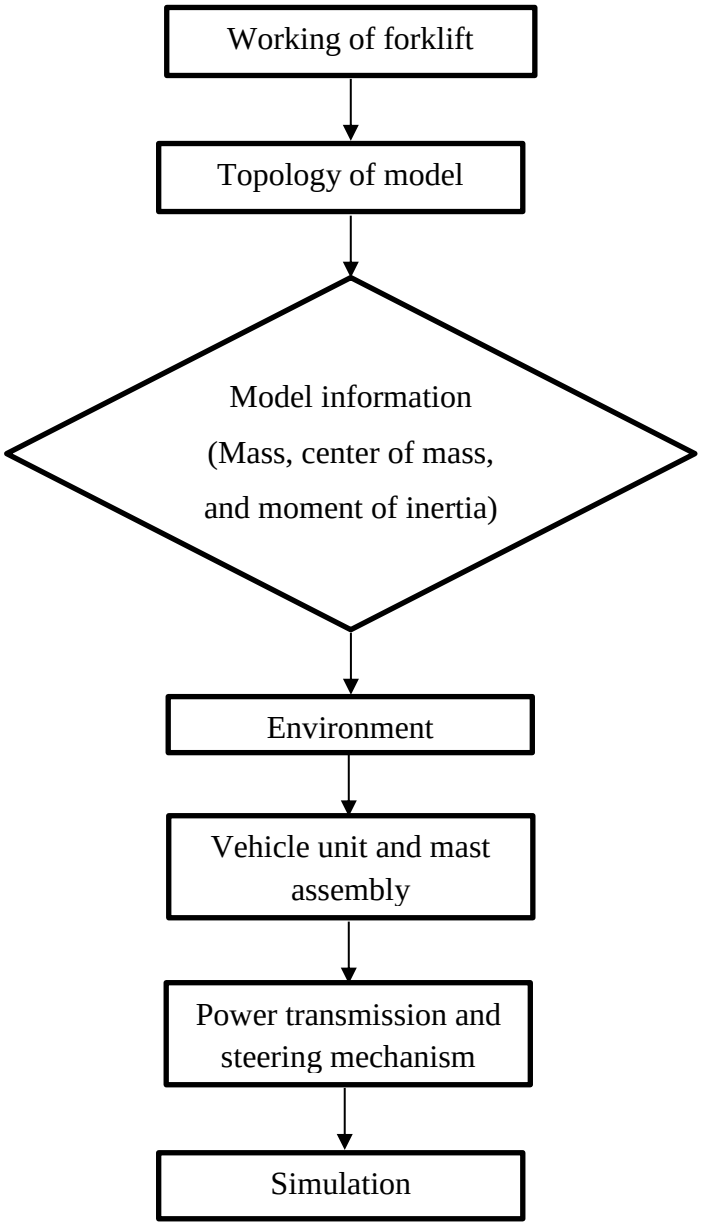

Figure 11. Mevea model tree of forklift

3.1 Working principle of forklift model

A forklift is considered a powerful tool to load, transport and un-load the heavy loads with a little effort of one person. The counterbalance forklift is type of truck in which extra mass is attached at the rear of vehicle unit to increase the lifting capacity. (Hangcha Group, 2011, pp. 59-75) The electrically powered counterbalance truck under study has three-wheels, 3.5 tons weight, lifting capacity of 2000 kilogram (kg), and speed 16 kilometer per hour (km/hr) also known as 3-wheel drive 2.0-ton forklift is shown in figure 12.

Figure 12. Electric 3W counterbalance forklift model

The counterbalance forklift enables efficient and smooth material handling between different stations in many industries (Hangcha Group, 2011, pp. 59-75. The load lifting vehicles are available in various sizes, lifting capacities, and power mechanisms. As discussed earlier, the vehicle unit of forklift is responsible for movement from one place to another and could be compared to a small truck whereas the mast assembly can lift the weight to several feet. Nevertheless, the speed of forklift is much less than truck but the working mechanism in most cases is same. The counterbalance forklift is powered with heavy electric motors for driving purpose. The electric motor could be either AC or DC. The electric motors with gearbox and planet gears power the front axle to move in forward and reverse direction. The

steering operation is performed by another electric motor so that the vehicle unit could turn around at specific angles. (Panara et al., 2015)

The mast assembly is supported by the vehicle body so that mast could tilt in forward and backward directions. The mast assembly of the counterbalance forklift under study consists of outer mast, inner mast, fork carriage and forks. The tilting operation is controlled by hydraulic cylinders and pistons and the outer mast normally can tilt up to 6° in both directions. The inner mast might be raised and lowered by single acting hydraulic actuators. The up and down movement of fork carriage can also be controlled by double acting hydraulic actuators and the both forks can move left and right with the help of hydraulic actuators. (Roux, 2015.)

3.2 Body components and topology of model

In order to build Mevea model, it is necessary to understand the basic components, connections and the functions in details. Basic components counterbalance forklift had already been described in early part of study. Vehicle unit has been illustrated in much detail. To explain the connections between vehicle unit and other parts of forklift, it is considered vital to discuss mast assembly components and connections.

The mast assembly portion is the complex portion of forklift having outer mast, inner mast, mast support, lift bracket, tilt bracket, hydraulic cylinders, pistons, pipes and hoses, pulley and chain mechanism, lift, and tilt rollers shown in figures 13a and 13b. The working of mast assembly will be explained from figures 13a and 13b. The vehicle unit could be connected and disconnected to mast assembly at outer mast through pins.

Outer mast could be fixed and rotated relative to the vehicle body at certain angle depending upon the design following the hydraulic cylinders and pistons movement shown in figure 13a. Figure 13b shows that inner mast can move in up and down directions with respect to outer mast. The relative motion of inner mast to outer mast could be controlled via pulley and chain and rollers for smooth motion. Inner mast is also attached to hydraulic cylinder and piston for movement in some designs. (Toyota Parts, 2017; Luciano Mondani, Mark Dodd, 2003; ProLift, 2017)

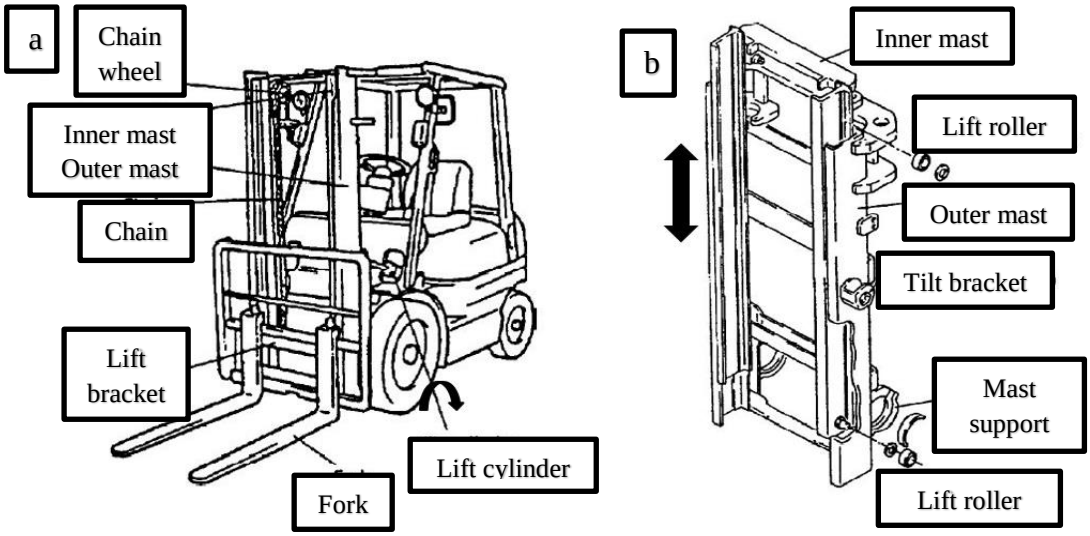

Figure 13. Mast assembly and its parts (ProLift, 2017)

Figure 14 describes how the fork carriage connects to inner mast and forks. The fork carriage is attached to inner mast with the help of rollers so that it could move up and down to lift load accordingly as shown in figure 14a. The load is to be lifted up by the forks which are assembled to fork carriage so that both forks might reciprocate in sideways together which is mentioned in figure 14a whereas figure 14b represents the detachable forks. The distance could be varied depending upon the application. (ProLift, 2017; Luciano Mondani, Mark Dodd, 2003)

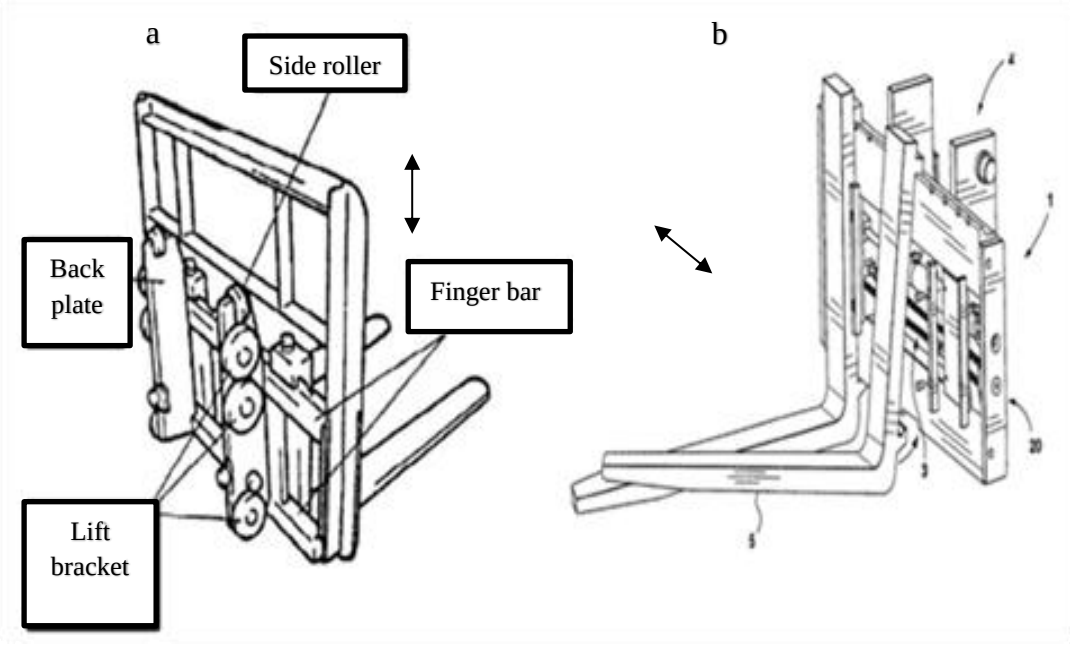

Figure 14. Fork carriage and forks (ProLift, 2017; Luciano Mondani, Mark Dodd, 2003)

The forklift modelling is started by listing the useful components of forklift, joints, and operations. The basic elements of forklift body are frame, overhead guard, counterweight, side covers, driver cabin, rear axle, rear wheels, front axle, front wheels, outer mast, inner mast, fork carriage, and forks. Rotational joints can be taken into account between vehicle unit and wheels. Brake system will be attained in simulated vehicle via wheels. Longitudinal and latitudinal frictions will be considered to describe the behavior of tires with road.

It could be inferred from literature review and discussion that mast assembly of forklift under study is the most complex part. It can rotate within specific angle range. Inner mast and fork carriage can move the loads up and down. Therefore, outer mast could be attached to vehicle unit via revolute joint. Inner mast is connected to outer mast with a translational joint. Fork carriage is also coupled to inner mast via translational joint. However, forks can be detached to fork carriage through pins and are moved in sideways when needed.

The listing down of components and movements relative to each other enable to draw topology of model. The simple structure represents the basic functions of all necessary components and helps in efficient and quick modelling on Mevea software. Topology of forklift model indicated in the figure 15 has been developed based upon the working principle of forklift.

To simplify the model and reduce the total number of bodies, few components of the model are joined together and taken as one body. The main body represented in figure 15 contains frame, overhead guard, counterweight, side covers, and driver cabin. Main body is connected to front and rear axles by revolute joints. Front axle enables the vehicle to move in forward and backward directions via wheels visible with black color circles in the figure 15. The revolute joint between rear axle and rear body would let the vehicle to steer within specified angle range. This revolute joint is provided for steering mechanism of Mevea model but the reference forklift is equipped different mechanism. The tilting of outer mast is due to the revolute joint between main body and outer mast. Translational joints represented in figure 15 let the inner mast and fork carriage to move up and down relative to outer mast and inner mast respectively. The forks can move due translational joint between forks and fork carriage.

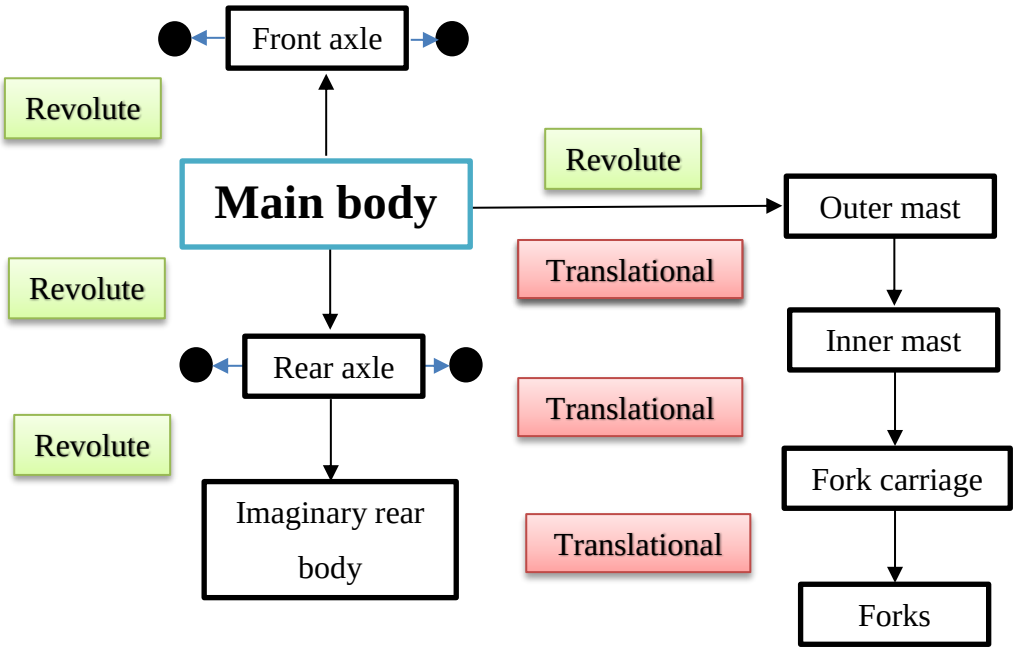

Figure 15. Topology of forklift model

3.3 Collecting model information

The next step in the modeling approach on Mevea software is to collect information of related components which are described in topology of forklift. For instance, the graphics of bodies must be designed in a suitable file format. Graphics of bodies in forklift Mevea model were converted to .3ds format. Each body requires mass, position, moment of inertia, and center of mass to be defined on Mevea software. This sort of data was written on excel sheet and the details of few of these will be mentioned in the end of report. As the information regarding the constraints has already been discussed in much details in topology of model so it was considered to estimate data regarding the range of outer mast tilt angles, inner mast, fork carriage and forks translational forces. Data on motor, friction, and braking splines were also written on excel sheet. To validate the model, the forklift speed, brake, tilt angles, speed of inner mast and fork carriage, and tilting angles of outer mast are taken from the physical prototype testing of reference forklift and will be compared to the simulation results in the later part of study.

3.4 Environment

Two types of environment models are available in Mevea known as gravel pit and flat terrain. The flat terrain model contains the sky graphics and has dome like shape. (Esa-Pekka Kaikko, 2015) The environment of simulation has been made based on weather conditions

and separate graphics available in Mevea software. The environment of current simulation contains sky, ocean, offshore port, ship, crane, containers, storage area and different loads represented in figure 16.

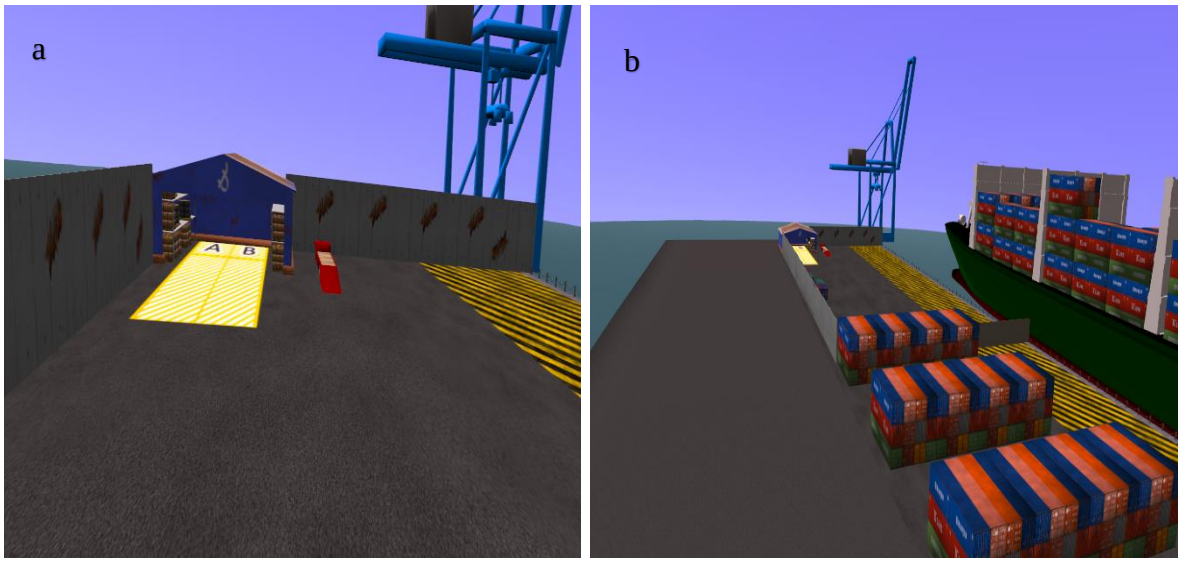

Figure 16. The environment of simulation

Figure 16a indicates the forklift in the storage area whereas the figure 16b explains the overall view of simulation. The flat terrain, dome shape and blue colored sky and ocean shown in figure 16 of simulation are taken from Mevea software. Environment components such as storage area, ground, containers ,and crane have been added to the simulation using respective graphics in .3ds format. The graphics of weights 700, 1000, 1500, 2000, and 2200 kg are also in .3ds format. For the purpose of better quality, the ship graphics are uploaded in .obj format. The forklift was planned to move in the storage area and load and unload the weights in storage area and containers. It might be possible that the user could throw truck in ocean while driving. Therefore, the fences are constructed around the boundary of seaport. All fence graphics are also taken in .3ds format.

3.5 Vehicle unit and mast assembly

The vehicle unit and mast assembly was modelled based upon the topology of model, information available in the literature review and reference forklift shown in figures 17a and 17b. In figure 17a, vehicle part being modelled on Mevea is shown. Mast assembly is described in figure 17b. As can be seen in figure 17a, the front axle has two tires at different positions whereas two tires are attached to rear axle. This type of truck is called 3 wheeled

forklift. The vehicle unit is replica of reference truck body. It is responsible for the movement of truck. An electric power transmission system is present in vehicle unit to assist the movement. Power transmission system will be described in detail in next chapter. Brake system is provided to stop the vehicle immediately at the hour of need. Longitudinal and latitudinal frictions between tires and road give the forklift a realistic feeling during motion.

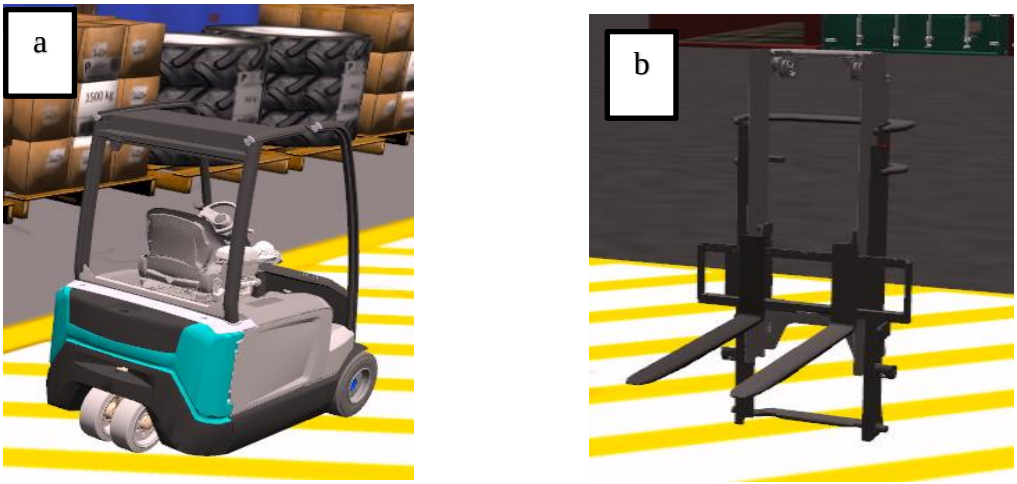

Figure 17. The vehicle unit and mast assembly

Figure 17b also indicates that the inner mast and fork carriage can move in upward and downward directions. It was considered better to avoid hydraulics which are responsible for movement of mast components. It could have consumed much time. Translational forces are utilized to limit and control the functions of mast. As already been described, it is connected to vehicle unit via revolute joint. Translational force-outermost has been used to limit the rotation of lifting part in the model. Motion was constrained with length instead of angles. The hydraulic cylinders and pistons are added as dummies in the model. Moreover, translational forces for inner mast, fork carriage and forks are included for the respective component functions. Movements of all components of mast are controlled with joystick.

3.6 Power transmission and steering operation

As discussed earlier, the front and rear axles are used for driving and steering purposes, respectively. Figure 18a and 18b explain the power transmission system needed to drive the vehicle in forward and backward directions. In the figure 18a, the front axle as power transmission had been shown. The driving mechanism is accompanied by an electric motor,

gearbox and planet gears present at both ends of front axles. The power transmission system of vehicle is further explored in the figure 18b. As can be seen in the figures, rear axle is not provided with any sort of electric motor for driving operation. Respective motor splines used to describe the motor torque against angular velocity are taken from reference forklift.

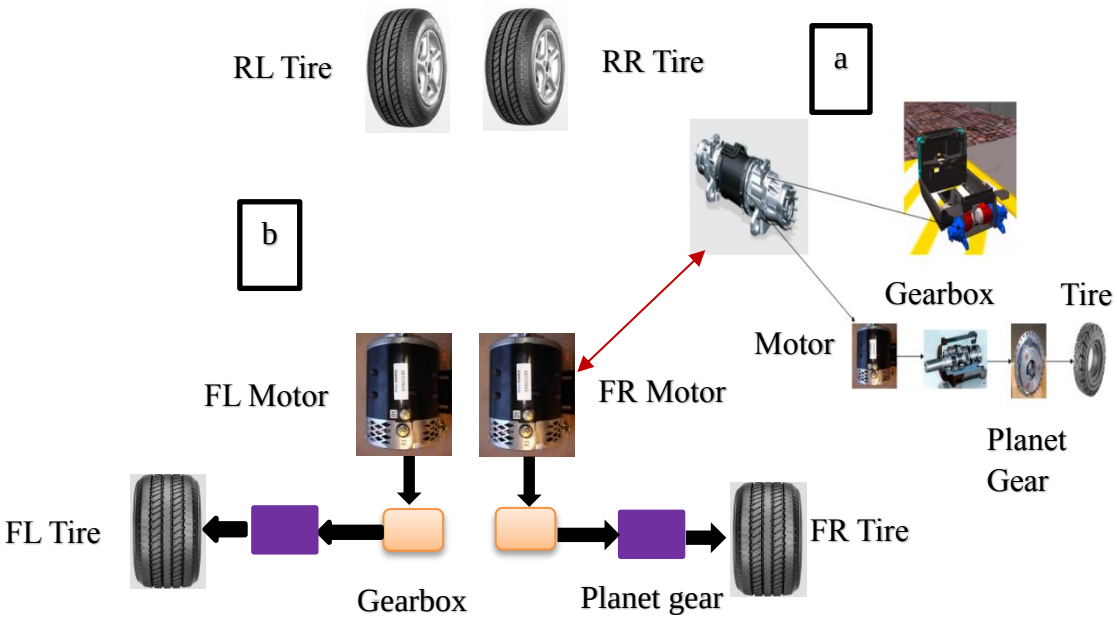

Figure 18. Power transmission of the vehicle unit

Electric motors connected to front axle are the reason for rear tires movement in the actual forklift. The reference counterbalance truck has only an electric motor at rear axle but it is used for steering operation. Steering electric motor is quite different from the driving motors. Power train consisting of two driving motors at front axle and no driving motor at rear axle was also tried on Mevea truck model. However, it was observed in simulated vehicle that the speed was much lower than demanded forklift. In order to increase the speed, various gear transmission ratios were utilized. None of the ratio enabled to achieve required speed limit probably due to inadequate transmission of motion to rear tires. Another possible solution of the problem was considered to use dummy motor and dummy planet gear at rear axle. Dummy motor and planet gears have transmission ratio 1. Again, the speed of model did not meet physical prototype results. It was noticed on Mevea model that dummy motor had rotated rear tires on different speed than front tires. Ultimately, it had also reduced the speed of vehicle. Therefore, this method could also not resolve the issue. Nevertheless, power transmission should have been transferred equally to rear tires as in front axle in both

cases but speed of vehicle on Mevea graphs was four times less than actual forklift. In order to confront this situation, identical planet gears as in front axle were used and attached to front motors. It ensured an equal motion transmission between front and rear axles. It could be noticed again that rear axle does not have any driving motor. Power is transmitted from front motors to rear axle via planet gears. The power transmitting train could be compared to actual forklift as explained in figure 18. It gave successful simulation speed results in real time. The speed of simulated vehicle was found identical to actual forklift.

The opted steering mechanism in simulation is shown in figure 19. An electric motor is used for rotating the rear wheels. As described in figure 19, motor can rotate the rear axle about y-axis so that torque is produced around x-axis. The forklift can turn within -85° and +85° angle range. For the sake of convenience, two forces were being used in the model to assist steering system of vehicle. Rear axle force was applied along y- axis and steering force was enforced perpendicularly. In result, a torque is produced around x- axis which let the vehicle unit to turn in the prescribed range. However, steering motor is used to achieve the purpose in later.

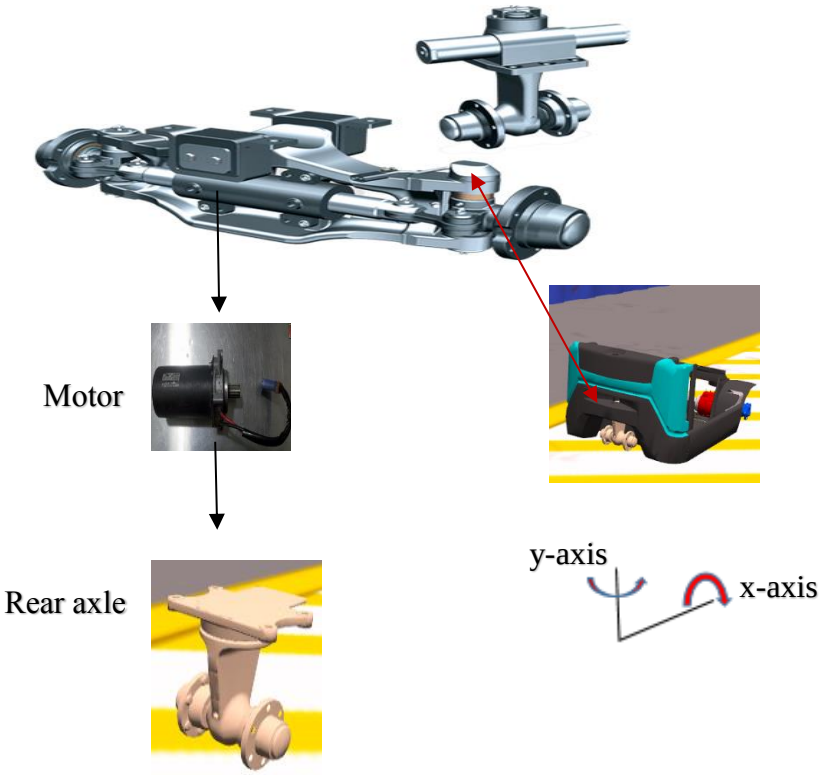

Figure 19. Steering mechanism of the vehicle unit

3.7 Simulated Mevea model

The final forklift model on Mevea software is shown in the figure 22. The movement of model is controlled by G 29 racing wheel and its accessories. The mast assembly is operated with Logitech joystick. The gearbox of the vehicle unit is automatic which means the forklift could move in forward and reverse directions. Digital buttons on the racing wheel are used to shift the gear box in forward and reverse modes. The vehicle could be accelerated in both directions using accelerator pedal and like normal truck the speed could be reduced using G29 brake pedal. The tilt operation of outer mast is managed with joystick in X direction whereas the lifting of inner mast is controlled in Y direction. The rotation of joystick about Z axis let the forks to move sideways. The fork carriage movement vertically is controlled by Logitech joystick.

It has been observed that the speed of vehicle was reduced while taking the turnaround curved path. The wobbling of mast was also seen during the movement which gives the model a realistic feeling. The forklift can uplift the weights up to 2000 kg without any problem. However, the weights more than 2500 kg cannot be lifted and more than 2000 kg could cause vibrations during lifting operation.

Figure 20. Simulated Mevea forklift model in real time

Final version of model was transferred to simulator. The input control and settings parameters on simulator are quite different than G29 racing wheel and Logitech joystick. Forward and reverse modes are changed with rocker buttons available on right side joystick. Vehicle body can be accelerated by right pedal whereas left one is used to stop simulated truck immediately. Steering wheel needed adjustments in input control parameters for turning the vehicle efficiently. Mast assembly operations are controlled with right and left joysticks of simulator. It was decided to rotate mast about z-axis using R-X joystick on simulator. Inner mast and fork carriage could be lifted with R-Y and L-Y joysticks, respectively. In 3 wheel 2.0 ton drive forklift, forks can be reciprocate in z-direction. Movement of forks are regulated using L-X joystick. Motion feedback is added to main body in y-axis on simulator so that realistic feelings could be experienced by users.

3.8 Mevea-Simulink Interface

Simulated forklift model is connected to MATLAB-Simulink for better controlling and optimizing the steering mechanism. Mevea software could be integrated to Simulink with the help of inputs and outputs signals. In the connection, Mevea software acts as the server whereas other software as host. Socket interface connects the software with Simulink via an IP address and port. S functions block of level 1 is debugged so that it has multiple inputs and outputs is used for communications in MATLAB. C code file of the function is converted into .mex and wrapper files for effective server-host connection.

Rear axle rotational angle, and angular speeds of rear, front right and front left wheels were chosen as output signals of Mevea software to Simulink as can also be seen in the figure 21. The rotational angle of real axle has already been defined in the range of -85° and +85°. Rate transition units convert transmitted data in optimal form in MATLAB. Steering mechanism model had already been developed on Simulink based on mathematical formulas. Distances of tires to the steering point of vehicle are taken into account to get the linear speed of vehicle. Steering mechanism subsystem performs mathematical operations on the Mevea data and speed of forklift is the final outcome of Simulink model. Again, the signals are converted into data signals via rate transitions which sends data back to the server. Mevea receives the signals as input signals. This process is repeated many times through the simulation time until the connection is established. Identical IP address and port numbers

are given in both simulation softwares. Time step needed for running simulations is kept same in the softwares.

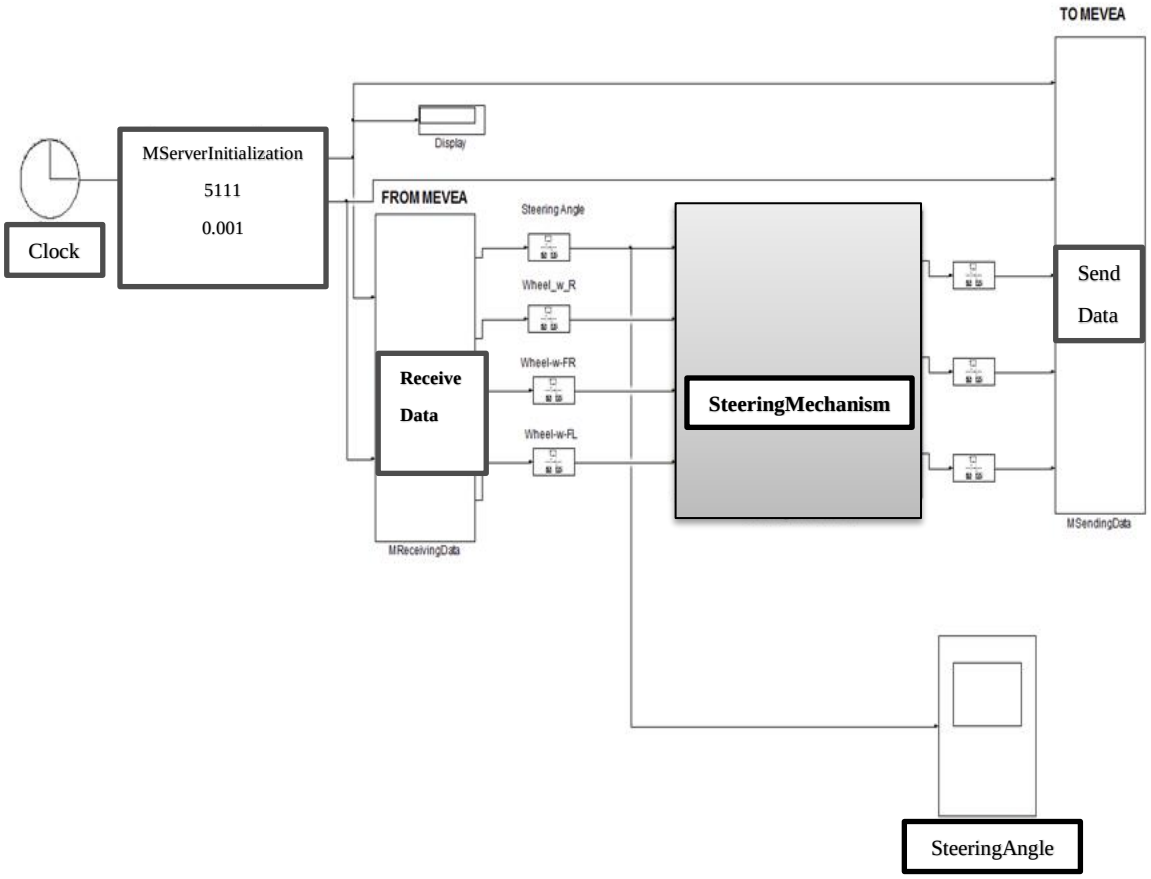

Figure 21. Simulink steering model

4 RESULTS AND MODEL VALIDATION

The working of forklift was tested using G29 racing wheel and Logitech joystick. The activities of vehicle and mast unit components of forklift was further verified with various graphs under different loading conditions. The speed-time, acceleration-time and steering operation are used to check the performance and efficiency of vehicle unit. The speed variations of reference forklift and simulated truck without load are shown in figure 22 with brown and blue line curves, respectively. Speed of forklift is measured in kilometer per hour as (km/h) indicated on vertical axis of graph whereas horizontal axis represents time taken in seconds (s). Speed-time graphs described in figure 22 is drawn when the accelerator pedal was fully pressed. Physical and virtual prototypes of forklift were moving in forward direction for the same duration of time.

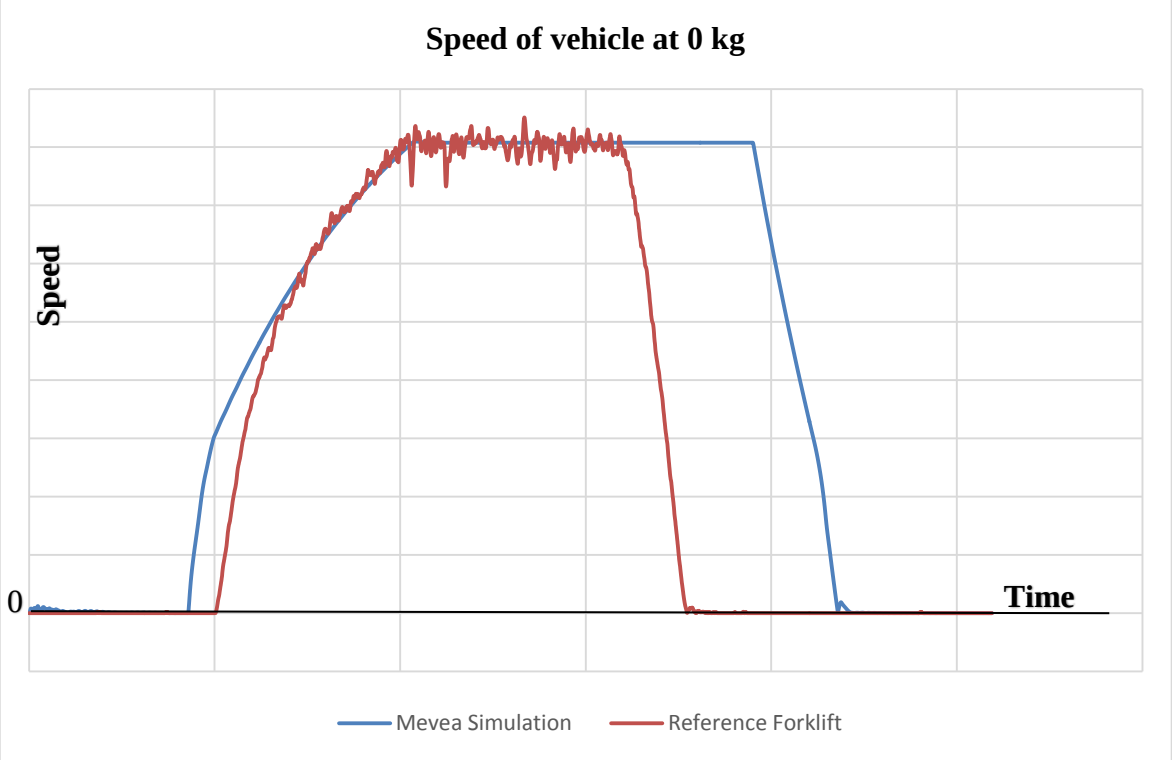

Figure 22. Speed of truck with 0 kg lifting load

Initial difference in the speed-time curves is due to fact that Mevea simulation was started before the actual forklift model. As can be seen in figure 22, brown and blue curves without any load increases significantly and reaches to maximum value. Speed-time graph of

simulated vehicle is slightly dissimilar in the beginning of curves. Blue curve shoots up abruptly as the accelerator pedal was pressed and reached to a value from where speed increases steeply with time. On other hand, brown line rises at constant rate with time. Simulated and actual vehicles gained exactly similar maximum speed in the corresponding duration of time. As the accelerator pedal was released, brown and blue lines fell gradually to zero value. Simulated blue curve indicates that pedal was released late. However, it could be seen both curves drop to minimum level at same rate. It declares that virtual and physical forklift models achieve the same maximum speed and travel identical distance when accelerator pedal was released.

Figure 23 illustrates the speed-time curves of reference and Mevea forklifts in 2000 Kg lifting load condition. As can be seen in the graph, brown line indicating actual truck speed is not identical to blue line. Brown curve goes up at higher rate whereas blue line climbs gradually with time and reaches to maximum speed. Top speed attained by reference of forklift is also slightly lower than Mevea model under 2000 kg load. When the accelerator pedal was released, brown color line declines abruptly. On other hand, blue line follows not different speed drop rate than in figure 22. It falls down with slightly higher rate. Speed-time graph of actual forklift shown in figure 23 also represents the effect of higher load.

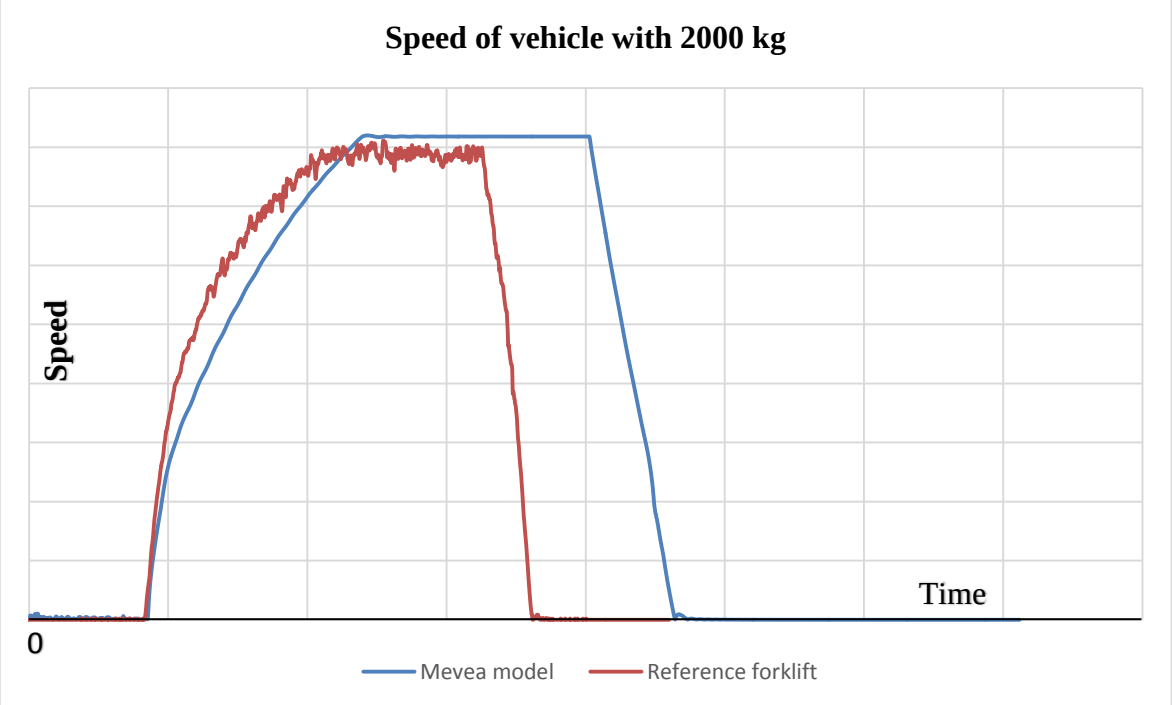

Figure 23. Acceleration of forklift with 0 kg and 2000 kg

In the figure 24, acceleration-time graph has been explained in the absence of any load. Acceleration is measured in kilometer per hour square (km/h^2) and time in s. As be seen in graph, acceleration of simulated vehicle starts from a constant value and gradually increases to maximum value. Conversely, brown color acceleration curve originates from a different acceleration and shoots up abruptly as racing pedal is pressed until it reaches to highest point. However, maximum acceleration achieved by reference and simulated forklifts are identical. When accelerator pedal was released, reference forklift acceleration curve suddenly plunges to a constant value whereas blue line falls to different value.

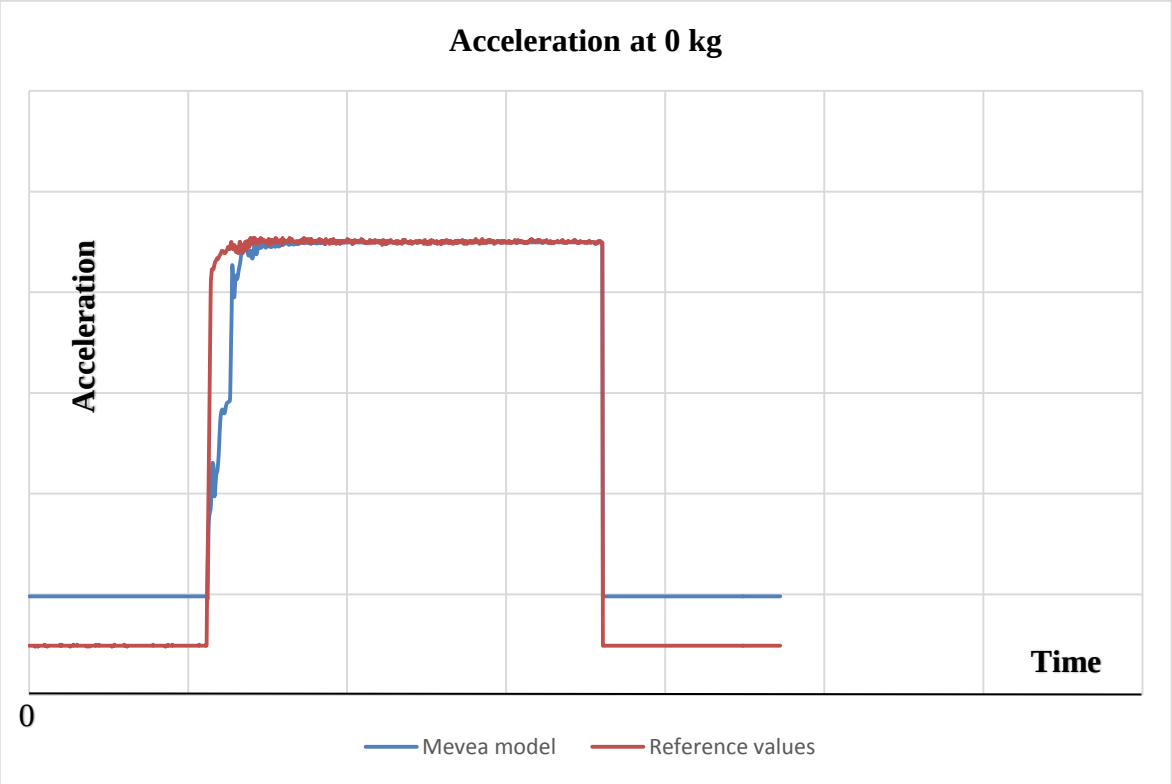

Figure 24. Acceleration of actual and simulated forklift model without load

Acceleration-time variations under 2000 kg load is shown in figure 25. Blue color line in the graph starts earlier than reference forklift curve as the accelerator pedal is pressed because of different recorded time. It rises sharply to highest acceleration. When the accelerator pedal was released, brown line drops to minimum constant value, immediately. The acceleration graphs for simulated and reference forklifts are identical except initial and final accelerations. Notice the very slight difference in acceleration-time curves is due to maximum lifting load.

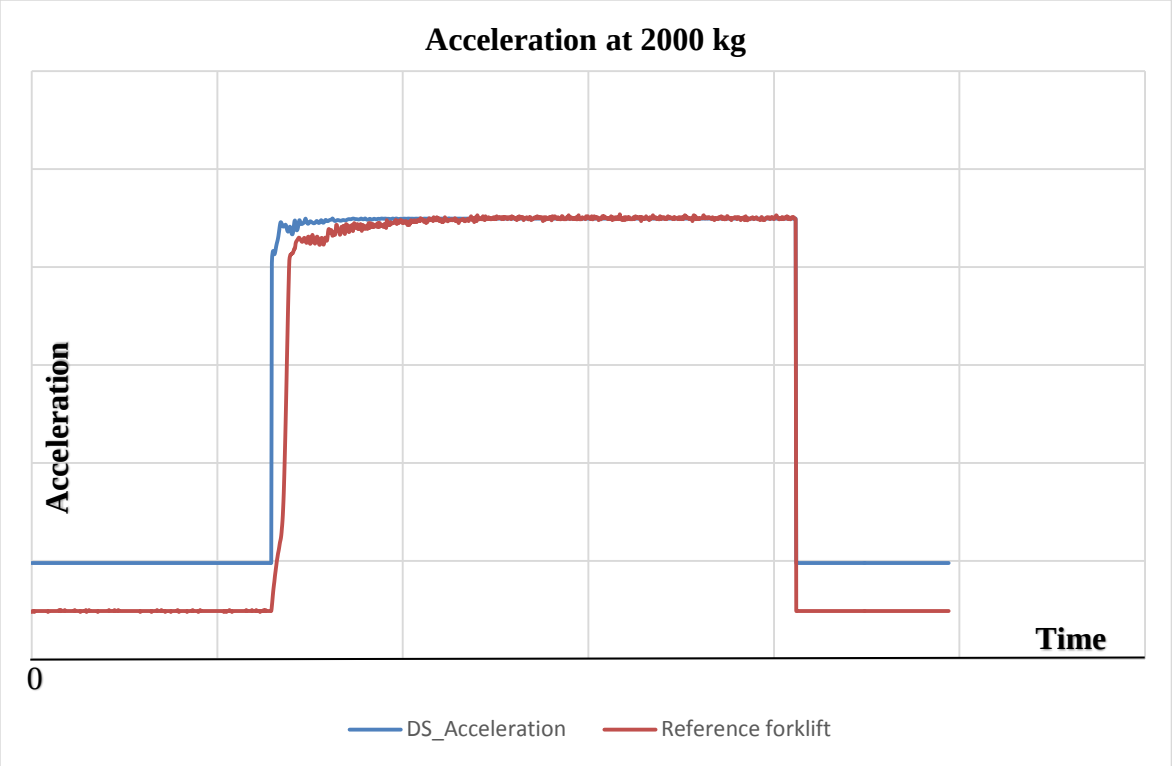

Figure 25. Acceleration of actual and simulated forklift model with 2000 kg load

As for as steering mechanism is concerned, vehicle unit can be turned between -85° and +85° and the performance of electrically powered steering system was observed by speed reduction around the curved path. It could also be witnessed in the actual forklift that the speed of vehicle reduces in the round path.

The performance of mast unit operations was analyzed using mast tilt angular speed, and various load lifting speeds. Fork carriage and inner mast move at similar speeds. Inner mast speed is taken into account to calculate the lifting speed. Tilting operation of simulated forklift mast was assessed by rotating outer mast with 0 kg and 2000 kg loads. Angular speed is considered as the parameter to investigate the performance of rotation. In figure 26, angular speed of outer mast has been illustrated with time. Upper black and lower black lines in the graph describe tilt speed in forward and reverse directions, respectively. As can be seen in figure, curve goes down initially representing tilt of outer mast in backward direction. Green color line oscillates at backward position about a mean point indicated as black line in the graph. The oscillations in graph are due to vibrations caused in mast unit after coming into rest at the end positions. Similar phenomenon could also been observed in reference forklift. It could also be termed as mast wobbling. Angular tilt speed remained same in

forward direction as well. Variations in the speed are identical in forward and reverse direction without any load.

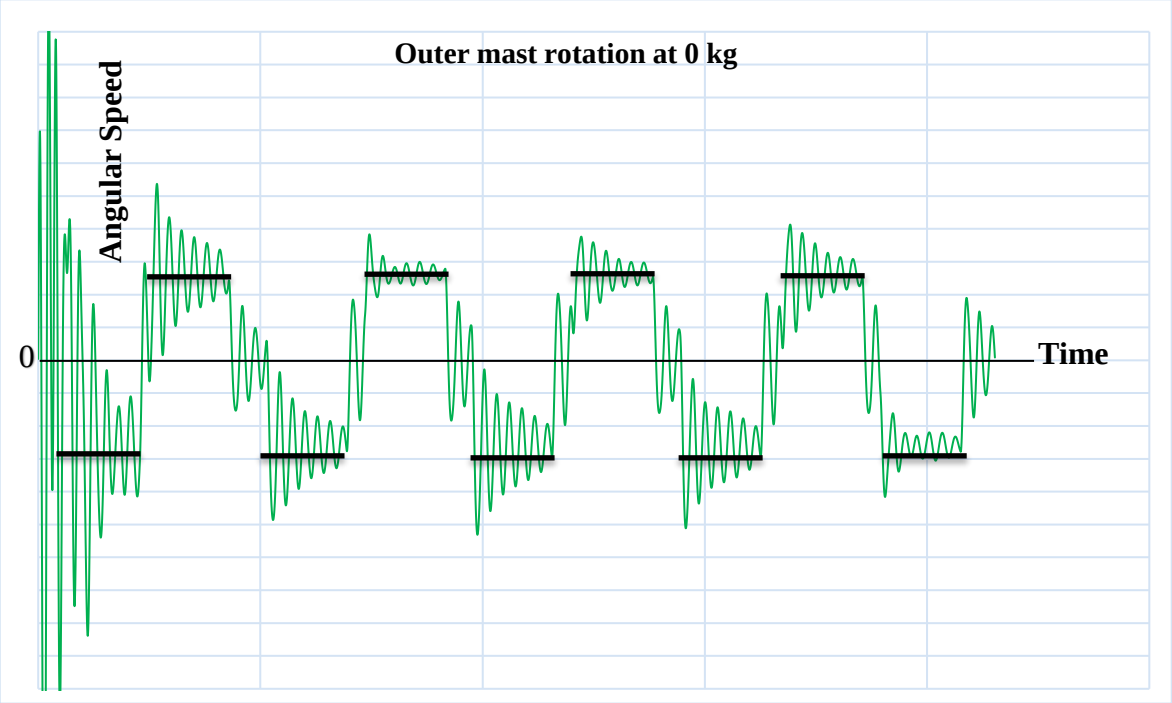

Figure 26. Outer mast rotation without load

In figure 27, tilt speed of simulated forklift outer mast in the presence of 2000 kg load have been represented. Outer mast vibrates with bigger amplitude in maximum loading case as can be seen with high peaks. Large oscillations about black lines are due to heavier lifting loads. However, angular tilt speed in forward and reverse direction is identical as the red line goes up and down at similar positions in the graph. In the graph 26, tilt speed in forward and reverse directions were also alike. It could be concluded from the results explained in figures 26 and 27 that tilt speed had kept same in both directions for 0 kg and 2000 kg loads in simulated vehicle. In comparison, actual forklift oscillates with slightly different tilt speed in forward and reverse directions. For 2000 kg load, actual forklift tilt speed was lesser than 0 kg load. On other hand, Mevea simulated mast assembly executed identical tilt speed for both loading conditions. Very slight variations in physical and virtual mast assembly could be due to fact that actual mast assembly are actuated with hydraulic system whereas forces are used to control the mast functions in the current Mevea simulation. However, very close mast wobbling effect was observed in actual and reference forklift. Therefore, tilt speed of mast in simulated and reference forklifts is almost identical.

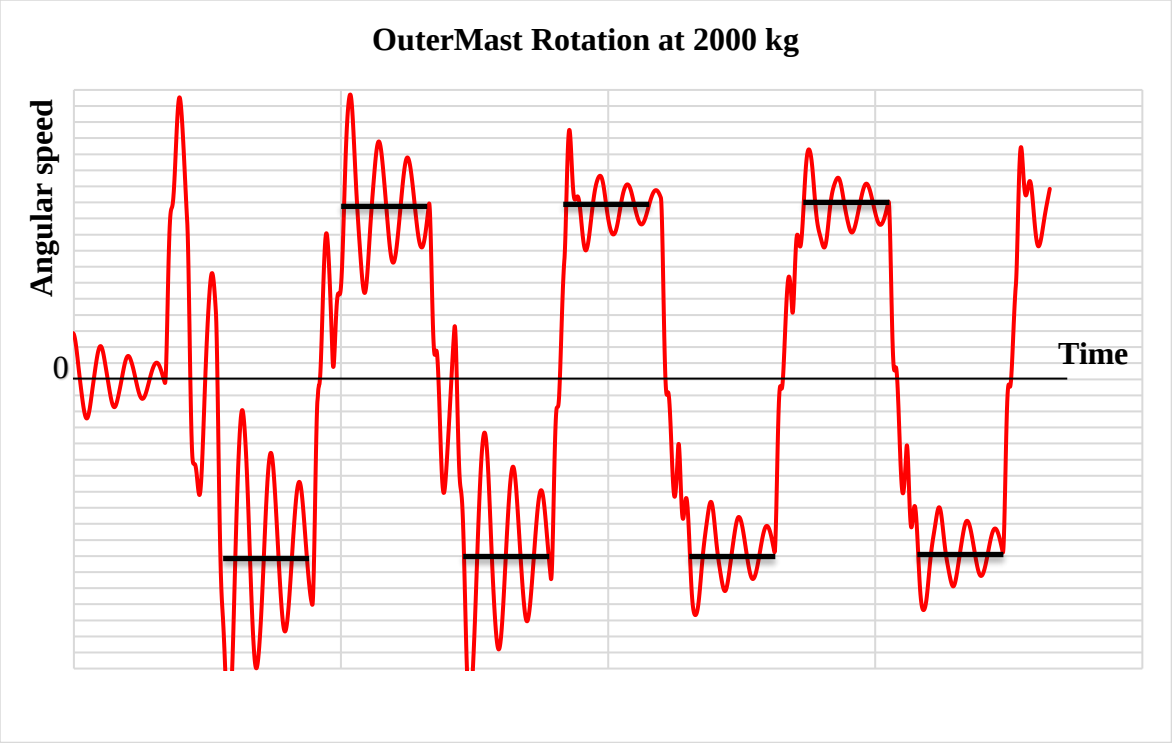

Figure 27. Outer mast rotation without load

To assess lifting operation of mast assembly 0 kg, 1600 kg, 1800 kg and 2000 kg loads were lifted. In the simulated forklift, inner mast and fork carriage are capable of lifting loads up and down at similar speed. Inner mast lifting speed is taken into account for the current measurements and would be compared to reference forklift mast lifting speeds for the intended loads. Lifting speed- time variations for no load could be seen in figure 28. Upper black lines show top positions whereas lower black lines indicate lower positions. The green color curve increases to maximum value and fluctuates around a constant value. Tendency of lift speed in downward direction is also similar as in upward direction. Lift speed- time graph shows similar changes throughout the time durations. Identical speed variations during lifting operation were recorded with reference forklift. Fluctuations in the graph are due to mast wobbling at the end positions. Reference forklift also represent the mast wobbling during lifting operations at upper and lower positions. Mast wobbling was also noticed in visual observations while controlling the inner mast movements with joystick. Graphical fluctuations confirm mast wobbling during load lift operations.

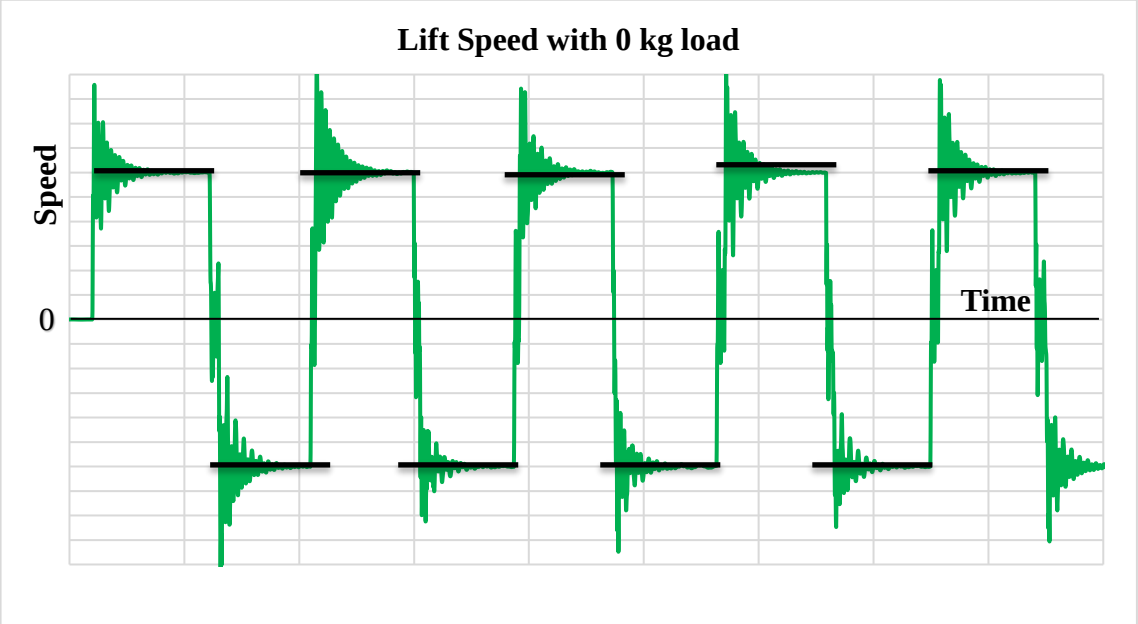

Figure 28. Lift speed with 0 kg load

In figure 29, lifting speed of inner mast under 1600 kg load is explained with blue color curve. Lift speed is alike in upward and downward directions. Also, mast wobbling effect could be seen at the upper and lower position. Note, in graph 29 mast wobbling is higher than in without any load.

Figure 29. Lift speed with 1600 kg load

Figure 30 describes lift speed-time graph of inner mast for 1800 kg load. Lift speed is same in upward and downward directions as in figures 28 and 29. In figure 30, mast oscillates with higher amplitudes at end positions than in previous observations of lift speed. Fluctuations indicate the effect of higher loads on mast function. It had also increased the mast wobbling phenomenon in mast components.

Figure 30. Lift speed with 1800 kg load

In the figure 31, the oscillations caused by the outer mast rotation under 2000 kg load has been indicated. There are few fluctuations at upward and downward positions. Fluctuations in the curves are much larger than the graphs indicated in the figures 28, 29 and 30. The possible reason for the fluctuations is the mast vibrations due to heavy load effect and wobbling phenomenon. However, after the fluctuations the curve indicates a constant line. The same trend is followed by the curve in next time intervals.

It could be noticed that mast lift speed in upward and downward directions are not different for lifting loads of 0 kg, 1600 kg, 1800 kg and 2000 kg. Physical prototype of forklift also indicated approximately identical lift speeds. Very slight variations in numerical values of actual forklift was observed due to heavy loads. On contrary, Mevea forklift lifting speeds

do not change with all loads. It was observed that forklift could lift to 2000 kg weight without any resistance. The vehicle body tilted up from rear between the range of 2000 kg and 2500 kg. When the loads more than 2500 kg were to be lifted the forklift was somersaulted.

Figure 31. Lift speed with 2000 kg load

5 ANALYSIS

Working of forklift model was tested using joystick and G29 racing wheels. The racing wheel accompanied with clutch and brake accessories were used to control the vehicle body movements. The digital buttons available on the racing wheel enabled to shift vehicle body in forward and reverse modes. The mast assembly operations are manageable with Logitech joystick. Outer mast could be tilted with joystick movement along X-axis and the load lifted up along Y-axis joystick movement. The user feelings such as speed, speed reduction around a curve, mast wobbling, loading lifting capacity of the model, and vibrations are observed on the desk and LUT SIM studio. The results of Mevea simulation are further compared with reference 3 wheel drive 2.0 ton forklift physical prototyping results.

Recall, the Mevea model speed-time graph presented in figures 22 and 23 the speed curves follow the same trend as with physical prototype results. The maximum speed gained by Mevea model from in the both graphs is also identical. It is evident in both graphs, the speed-time variations in 0 kg and 2000 kg lines shot up, follows the same peak values and go down at equal interval of times. Notice, heavy load had effect on physical prototype speed. It increases at higher rate than with 0 kg loading condition. In comparison, simulated truck model speed graph follows the exactly same variation as without load.

In figures 24 and 25, the acceleration-time graph in 0 kg and 2000 kg obtained from virtual and physical prototypes testing of reference forklift are shown. The acceleration-time line for both cases goes up when the accelerator pedal was pressed. The curves reach to identical constant line of maximum acceleration. As the accelerator pedal was released the brown color lines drop immediately to a constant value in 0 kg and 2000 kg loading conditions. In the case of simulated vehicle, the acceleration curves originate and end to a different value than the reference forklift. It could also be seen in prototype tests the acceleration lines drop quickly when accelerator pedal was released. The effect of maximum load which could be lifted by truck on acceleration-time graphs is quite similar in the simulation and prototype results.

As for as the steering mechanism in reference forklift is concerned it has been observed that the speed of actual forklift reduces and becomes constant during turning operation of vehicle around a curved path. However, in the Mevea simulation of 3 wheel drive 2.0 ton forklift the speed only reduced. It never became constant during steering operation.

Mast assembly functions showed a slight different behavior than reference forklift. For instance, outer mast tilt speed remained unchanged in forward and reverse directions in simulated forklift case. On contrary, very small decrease in tilt speed of physical prototype was recorded with 2000 kg. However, tilt speed forward and backward was identical in 0 kg load for actual forklift. Heavy load and mast wobbling effects in 0 kg and 2000 kg cases are comparable to actual and simulated forklifts. Lift speed in upward and downward directions remained unchanged with 0 kg, 1600 kg, 1800 kg and 2000 kg loads in simulated truck model. In each lifting case, the lift speed is found different in up and down direction for reference forklift drive. It was decreasing with the increase of load.

By comparing the results, it could be seen that Mevea model of forklift had gained most of objectives. The simulated model has same lifting capacity of 2000 kg as the physical prototype. The maximum speed and acceleration achieved by forklift without and 2000 kg load is also identical. However, slight variations in acceleration-time graphs of actual and physical prototypes are observed. Identical angle parametric range could be set for steering truck. Speed of vehicle is reduced while taking turn. Developed vehicle unit model is quite close to 3 wheel drive 2.0 ton forklift vehicle unit.

As for as working of mast is concerned, some minor differences such lift speed of inner mast have been noticed in taking up various loads. It was seen that physical prototype had tendency of reduction in lift speed with huge loads. Conversely, simulated forklift model showed lift speed in upward and downward directions. Hydraulics could have improved mast assembly functions much effectively if introduced. In order to save time, it was considered to utilize only the translational forces to limit actions of components in a defined range. However, fluctuations on the lift speed-time graphs represent heavy load feelings and mast wobbling effects. Angular speeds of outer mast along z-axis also remained unchanged for simulated forklifts whereas reference forklift values change for different loads.

At the moment, user feelings speed reduction around a curve, mast wobbling, loading lifting capacity of the model, and vibrations during lift were achieved to some extent. Some outcomes of user feelings could also be seen in the simulated generated graphical results. Visual effects are added in the simulation and users had confirmed while working with model on desk and on simulator.

It was mentioned in the beginning of study that virtual glasses and leap controllers could be added to the simulation to achieve realistic feelings. Unfortunately, Mevea software currently does not support virtual glasses due to few technical updates. Therefore, virtual glasses and leap controller related material had not been added in much details. Considering the simulation graphical results, user feelings, and experience on simulator it could be said to some extent that developed model is the real time simulation forklift model developed by Mevea. It could be further used to make important and abrupt changes in design.

6 CONCLUSION

The main objective of research is to build real time simulation of 3 wheel drive 2.0 ton forklift using Mevea software. It was expected that simulated Mevea model would be identical to reference forklift in terms of visualization and graphical results. Visual features of simulation could be added to model as user feelings to increase realistic impressions. Speed-time, acceleration-time, lift speed-time, and rotational speed-time are considered graphical results which would be compared to physical prototype tests. Developed model was expected to strengthen R&D department so that quick changes could be made in design with minimum effort. Hence, it would save considerable cost, effort, and time in product development needed by conventional methods require to manufacture physical prototype for mechanical testing.

The research problem under discussion was further split into three questions: development of model, real time simulation and control, and attachment of virtual reality tools. Topology of model and collected information related to physical prototype let to build a functional counterbalance truck model on Mevea software. Realistic features are added to model in terms of mast wobbling, heavy load feelings, speed reductions around curve, collisions and climbing the vehicle over a slope. These user feelings were obtained by adjusting input parameters and spring and damping constants of modelling forces available in Mevea software. Simulation model was controlled via G 29 racing wheel and joystick. It was planned to integrate simulation model with virtual glasses, leap controllers, and simulator to feel the realistic behavior of model.

Generated Mevea model is working properly at the moment. Functional parameters such as speed of vehicle unit, brake system, steering mechanism, outer mast rotation, lift speed, lift capacity are replica of reference forklift to some extent. The maximum speed and acceleration gained by simulated forklift is identical to actual counterbalance truck and speed of vehicle is also decreased in steering operation.

Brake system response is also comparable to real truck. Simulation model can lift maximum load of 2000 kg like 3 wheel drive 2.0 ton actual forklift. There is slight variations in lift

speed while taking up loads of different weights in actual truck model. However, the simulation model has same lift speed in upward and downward directions. Outer mast rotational speed values also remain unchanged for Mevea model. It is observed angular speed of mast was dissimilar with 0 kg and 2000 kg loads in reference forklift. As for as user feelings are concerned, mast wobbling and heavy load feelings are observed by users on desk and simulator. These features could also be seen in actual counterbalance forklifts. Working of model was controlled with joystick and G29 racing wheel. Virtual glasses are not supported by Mevea at the moment. Therefore, it was considered to skip virtual glasses and leap controllers. In order to experience real time user feelings, simulated vehicle is further transferred to simulator and motion feedback let the user to feel the virtual reality.

Deviations in mast assembly results could be noticed are the outcomes of translational forces being used to actuate the mast components. In actual forklift, these components are moved by utilization of hydraulics. Therefore, slight variations in simulated and prototype results could have been removed if hydraulic options available in Mevea were utilized instead of forces. Further, real time results could be achieved if Mevea-Simulink interface based on hydraulic equations were applied. Moreover, steering system could also be improved using Simulink interface.

Developed forklift model is the real time simulation model of forklift. Considering actual 3 wheel drive 2.0 ton forklift technical specifications and simulated model specifications, it could be concluded that Mevea model is the replica of reference forklift. However, very slight differences in few observations could have improved with little effort on hydraulics and Mevea interface with other computational softwares. Added user feelings in the model are the key specifications which has made model as real time simulation. Furthermore, the exposure of simulated forklift to virtual reality tools let the users to experience wonders of forklift real time simulation using Mevea software.

Mevea modelling enables R&D department to make very quick changes in the model at very low cost. It eradicates the fear of physical prototype testing failure. Re-manufacturing of physical prototype could be forgotten. Advanced multibody system Mevea software let R&D people to visualize and examine changes on the personal computers with little effort. Expertise level of R&D people is not important in virtual prototyping approach. Mechanical

engineers having less knowledge on electrical components and power transmission system could take decisions in minimum time. Even the customers having no technical background can participate in product development process. In short, Mevea software is an extraordinary product development tool in modern world. .

REFERENCES

Baharudin, M. (2016). Real time simulation of multibody systems with applications for working mobile machines. [online] Acta Universitatis Lappeenrantaesis 690(ISBN 978-952-265-932-3), pp.24-43.

Bermejo, A. and Felez, J. (2016). Design of an anti-tip over control for counterbalance forklifts using bond graph models.

Bruno, F., Caruso, F., Li, K., Milite, A. and Muzzupappa, M. (2008). Dynamic simulation of virtual prototypes in immersive environment. *The International Journal of Advanced Manufacturing Technology*, 43(5-6), pp.620-630.

Davis, R. (2013). A guide to forklift operator training. *ASME Standords*.

Hangcha Group, C. (2011). *1t-3.5t R Series Internal Combustion Counterbalanced Forklift Truck*. 1st ed. [ebook] China: HANGCHA GROUP CO., LTD., pp.59-75. Available at: http://www.forklift.ee/files/spec_5320_469.pdf.

Kaikko E.P (2015). *Development of generic simulation model for mobile working machines*. Master Thesis. Lappeenranta: Lappeenranta University of Technology, pp.49-50.

Karkee, M., Steward, B., Kelkar, A. and Kemp, Z. (2010). Modeling and real-time simulation architectures for virtual prototyping of off-road vehicles. *Virtual Reality*, 15(1), pp.83–96.

Luciano Mondani, Mark Dodd (2003). *Fork movement assembly for lift trucks*. US20030156935 A1.

Panara, K., Mishra, V., Patel, A., Patel, T. and Dhivar, K. (2015). Construction of Battery Operational Forklift. *International Journal of Science Technology & Engineering*, [online] 2(4), pp.127-131.

ProLift, F. (2017). *Types of Forklift Uprights and Masts*. [online] Proliftequipment.com. Available at: http://www.proliftequipment.com/blog/2014/12/11/types-of-forklift-uprights-and-masts/ [Accessed 11 May 2017].

Roux, F. (2015). *Free lift mast for truck mounted forklift*. US 8777545 B2.

Tiainen, T., Ellman, A. and Kaapu, T. (2014). Virtual prototypes reveal more development ideas: comparison between customers' evaluation of virtual and physical prototypes. *Virtual and Physical Prototyping*, 9(3), pp.169-180.

Toyota Parts. (2017). *Toyota parts diagram forklift | Equipment guard from forklift | Forklift 3 stage*. [online] Tentheypo.strefa.pl. Available at: http://tentheypo.strefa.pl/toyota-parts-diagram-forklift.html [Accessed 11 May 2017].

APPENDICES

Appendix 1: Bodies positions, masses, center of mass and moment of inertia

A= 1.14 m

B= 1.695 m

C= 2.125 m

D= 2.079 m

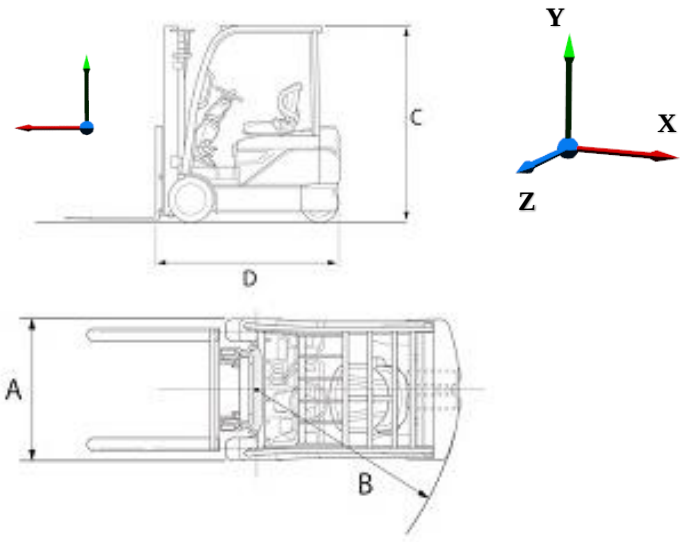

1. Main Body

Mass (kg)	**2761**		
Position (x,y,z)	**44**	0.2	-10
Center of mass (x,y,z)	**-1**	0	-0.07

Moment of inertia

500		
	500	
		750

2. Rear Axle

Mass (kg)	**300**		
Position (x,y,z)	**-1.422**	-0.01	0
Center of mass (x,y,z)	**-1.39588**	0.13	0.0035

Moment of inertia

40		
	70	
		55

3. Outer Mast

Mass (kg)	**117.1**		
Position (x,y,z)	**0.125**	-0.125	0
Center of mass (x,y,z)	**0.1425**	1.012	0.004

Moment of inertia

60		
	10	
		66

4. Inner Mast

Mass (kg)	**117**		
Position (x,y,z)	**0**	1.3	0
Center of mass (x,y,z)	**0.0858**	1.432	-0.007

Moment of inertia

60		
	10	
		65

5. Fork Carriage

Mass (kg)	**101.3**		
Position (x,y,z)	**0**	-0.9	0
Center of mass (x,y,z)	**0.191**	0.21564	0

Moment of inertia

27		
	35	
		45

6. Forks

Mass (kg)	**78.4**		
Position (x,y,z)	**-0.025**	-0.563	0
Center of mass (x,y,z)	**0.6775**	0.01	-0.001

Moment of inertia

15		
	22	
		25

7. Front Tire

Mass (kg)	**178**		
Position (x,y,z)	**0**	0	0.5 or -0.5
Center of mass (x,y,z)	**0**	0	0

Moment of inertia

14		
	14	
		45

7. Rear Tire

Mass (kg)	**64**		
Position (x,y,z)	**0**	0	-0.115 or 0.115
Center of mass (x,y,z)	**0**	0	0

Moment of inertia

5		
	5	
		25

Appendix 2: Power transmission

1. Motor spline

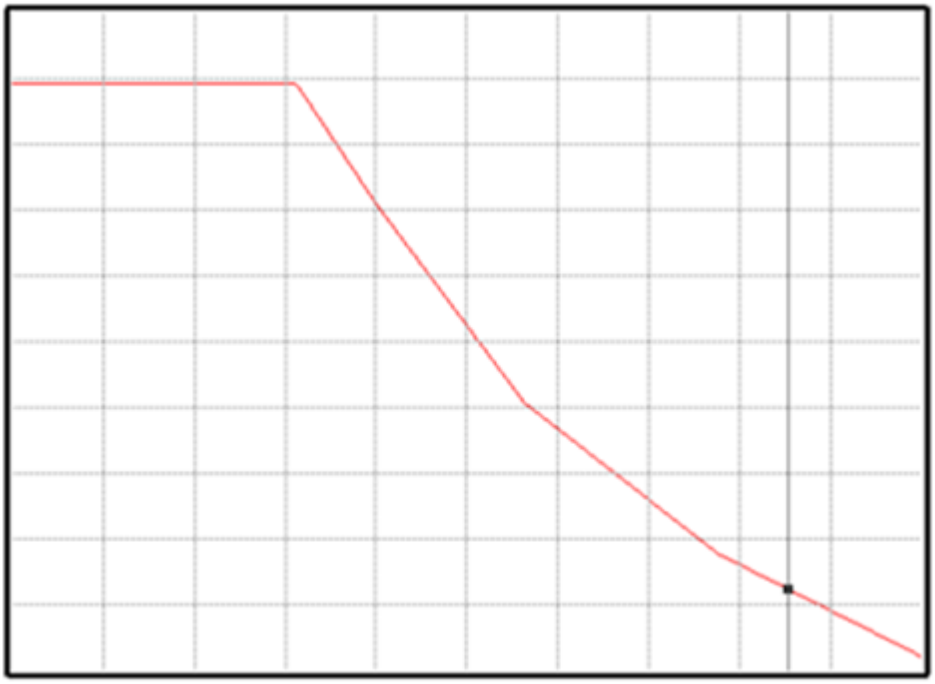

2. Brake spline

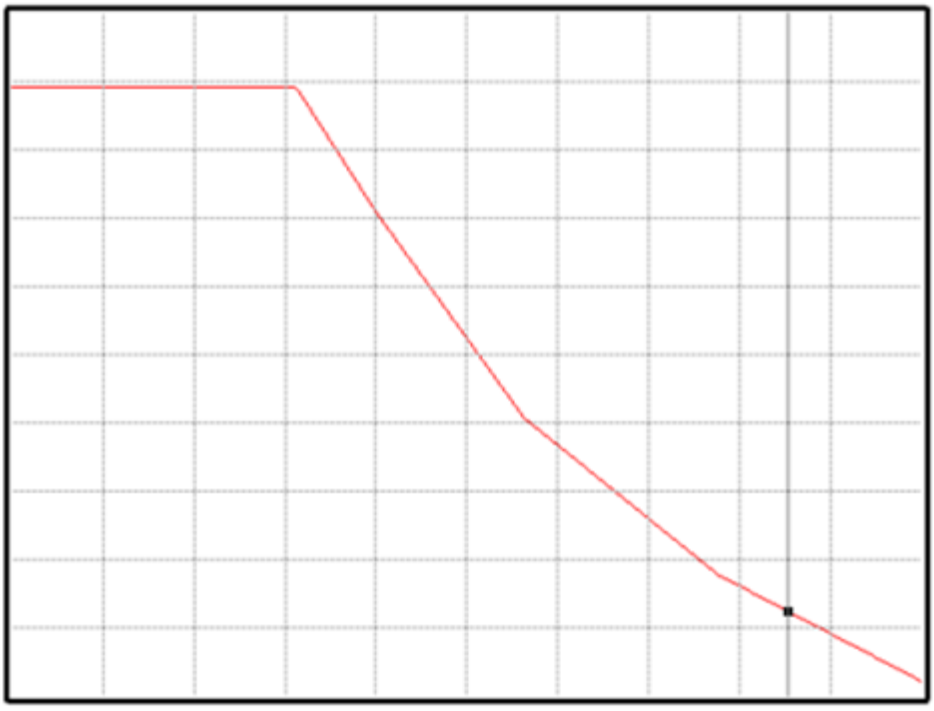

3. Longitudinal Friction

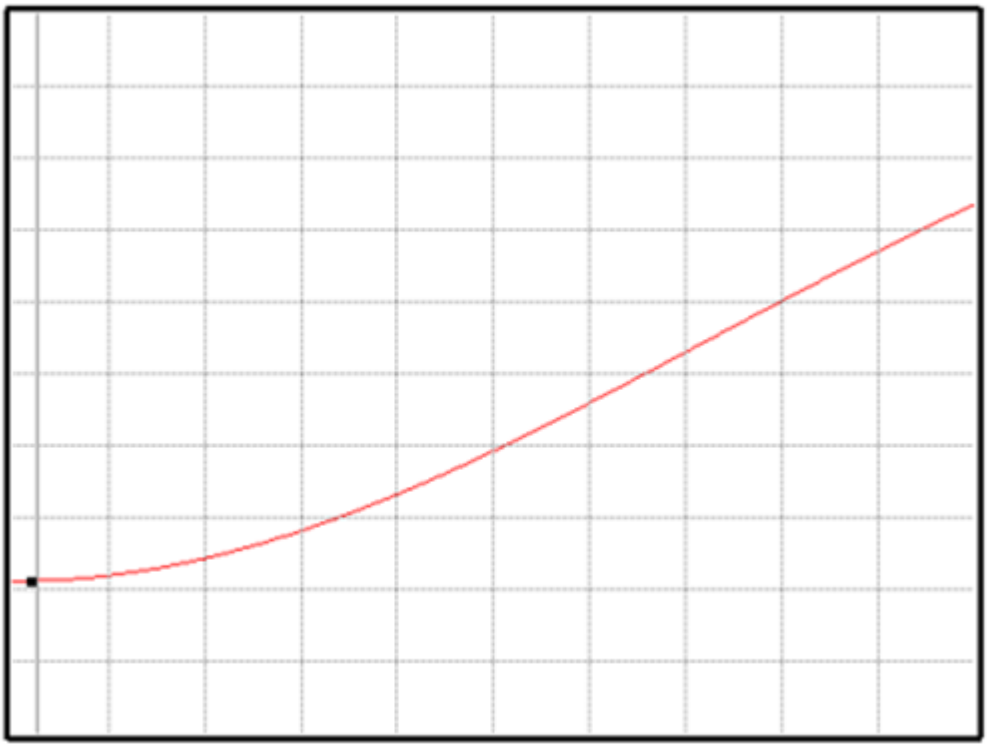

2. Latitudinal Friction